INSTITUTO SUPERIOR DE ENGENHARIA DO PORTO
MESTRADO EM ENGENHARIA MECÂNICA




WOOD-STEEL CONNECTIONS (W-S-W) IN DOUBLE SHEAR AT ROOM AND HIGH TEMPERATURES

LINO DANIEL SOARES SILVA
novembro de 2019

POLITÉCNICO
DO PORTO

WOOD-STEEL CONNECTIONS (W-S-W) IN DOUBLE SHEAR AT ROOM AND HIGH TEMPERATURES

Lino Daniel Soares Silva

2019
ISEP – School of Engineering
Department of Mechanical Engineering

POLITÉCNICO
DO PORTO

WOOD-STEEL CONNECTIONS (W-S-W) IN DOUBLE SHEAR AT ROOM AND HIGH TEMPERATURES

Lino Daniel Soares Silva
1141235

Dissertation presented to ISEP – School of Engineering to fulfill the requirements necessary to obtain a Master's degree in Mechanical Engineering, carried out under the guidance of Doctor Elza Maria Morais Fonseca.

2019
ISEP – School of Engineering
Department of Mechanical Engineering

POLITÉCNICO
DO PORTO

JURY

President
Doctor Raul Duarte Salgueiral Gomes Campilho
Assistant Professor, ISEP – School of Engineering
Supervisor
Doctor Elza Maria Morais Fonseca
Assistant Professor, ISEP – School of Engineering
Examiner
Doctor Paulo Alexandre Gonçalves Piloto
Full Professor, IPB – Polytechnic Institute of Bragança

ACKNOWLEDGEMENTS

First of all, I would like to thank Prof. Elza Maria Morais Fonseca for the unconditional orientation provided throughout the whole realization of the dissertation, through which was given me all the support, knowledge, advice and criticism necessary for its completion.

To my family, for always providing me with the necessary conditions and all the support from the beginning of my academic career.

A special appreciation to Anastasiya for all the support, constant encouragement and knowledge shared throughout the whole academic path.

KEYWORDS

W-S-W Connection; Dowels; Gypsum; Char layer; Fire; Thermal Analysis

ABSTRACT

The present master thesis was developed in Master's degree in Mechanical Engineering on the branch of Mechanical Constructions.

The main purpose of this thesis is to study the behavior of wood connections (protected and unprotected) of the wood-steel-wood type (W-S-W) under double shear, with dowels as connectors and a steel plate as central member at room temperature and high temperatures. For this, it was required to use an analytical and numerical method and, subsequently, its comparison was performed. The analytical method, based on simplified equations from Eurocode 5, parts 1-1 and 1-2, was used in order to design the mechanical and thermal behavior of wood connections with steel dowels. The numerical methodology, based on the finite element method with ANSYS Academic Mechanical® software, was used in order to obtain computational thermal simulations, which allow verifying the effect of the connectors, the steel plate and the gypsum boards on the char layer growing effect. The comparison between analytical and numerical methods provides additional information in order to certify designers and professionals that this type of connection is safe to use. For each studied connection, different dowel diameters and applied loads were used, both at room temperature and under fire exposure. Loads of 10, 15 and 20 kN were admitted, with dowels diameters of 6, 8 and 10 mm. The re-arrangement of the connectors was kept constant in three columns but different lines in all designed connections. Three different types of wood were used, GL20h, GL24h, and GL32h. The fire action in the connection was imposed by the standard curve ISO834. In the protected connections, two types of insulators were used, gypsum types A and F, in order to protect the connection during 60 min under fire conditions.

PALAVRAS CHAVE

Ligação M-A-M; Cavilhas; Gesso; Camada carbonizada; Fogo; Análise Térmica.

RESUMO

A presente dissertação foi desenvolvida no Mestrado em Engenharia Mecânica na área de Construção Mecânicas.

O objetivo fundamental da presente dissertação é estudar o comportamento de ligações (protegidas e não protegidas) do tipo madeira-aço-madeira (M-A-M) em corte duplo, com cavilhas e uma placa de aço como membro central, à temperatura ambiente e a elevadas temperaturas. Para tal, foram utilizados os métodos analítico e numérico e, posteriormente, foi realizada a comparação de valores. O método analítico, baseado em equações simplificadas apresentadas no Eurocódigo 5, partes 1-1 e 1-2, foi utilizado no dimensionamento mecânico e térmico das ligações de madeira com cavilhas. A metodologia numérica foi baseada no método dos elementos finitos, implementada no programa ANSYS Academic Mechanical®, de forma a obter simulações computacionais térmicas, que permitem verificar o efeito dos conectores, da placa de aço e das placas de gesso no efeito do avanço da camada carbonizada. A comparação de valores, entre os métodos analítico e numérico, fornece informações adicionais aos projetistas e profissionais certificando este tipo de conexões como seguras para uso. Para o projeto de cada ligação, foram utilizados diferentes diâmetros de cavilhas e forças aplicadas, tanto para o carregamento à temperatura ambiente como em situação de exposição ao fogo. Foram admitidas cargas de 10, 15 e 20 kN, com diâmetros de cavilhas de 6, 8 e 10 mm. A disposição das cavilhas foi mantida constante em três colunas, mas em função de cada ligação, o número de linhas poderá variar. Foram utilizados três tipos de madeiras diferentes, GL20h, GL24h e GL32h. A ação do fogo na ligação foi imposta pela curva normalizada ISO834. Nas ligações protegidas, foram utilizados dois tipos de isolamento, gesso tipo A e tipo F, de forma a proteger a ligação durante um período de 60 min sob ação do fogo.

LIST OF SYMBOLS AND ABBREVIATIONS

$f_{m,g,k}$	Bending strength (N/mm^2)
$f_{t,0,g,k}$	Tensile strength parallel to the fiber (N/mm^2)
$f_{t,90,g,k}$	Tensile strength perpendicular to the fiber (N/mm^2)
$f_{c,0,g,k}$	Compressive strength parallel to the fiber (N/mm^2)
$f_{c,90,g,k}$	Compressive strength perpendicular to the fiber (N/mm^2)
$f_{v,g,k}$	Shear strength (N/mm^2)
$E_{0,g,mean}$	Average modulus of elasticity parallel to the fiber (N/mm^2)
$E_{0,g,05}$	Modulus of elasticity parallel to the fiber (N/mm^2)
$E_{90,g,\,mean}$	Average modulus of elasticity perpendicular to the fiber (N/mm^2)
$E_{90,g,05}$	Modulus of elasticity perpendicular to the fiber (N/mm^2)
E_L	Modulus of elasticity along the longitudinal axis, wood (N/mm^2)
E_R	Modulus of elasticity along the radial axis, wood (N/mm^2)
E_T	Modulus of elasticity along the tangential axis, wood (N/mm^2)
ω	Moisture content
$\sigma_{t,0,d}$	Design tensile stress along the grain (N/mm^2)
$f_{t,0,d}$	Design tensile strength along the grain (N/mm^2)
k_{mod}	Modification factor for load duration and moisture content (-)
γ_M	Partial factor for material properties (-)
F_d	Applied design force (N)
A_s	Cross-section of the member (mm^2)
$F_{v,Rk}$	Characteristic load-carrying capacity per shear plane and per fastener (N)
$f_{h,1,k}$	Characteristic embedment strength in timber member (N/mm^2)
$M_{y,Rk}$	Characteristic yield moment of the fastener (Nm)
$F_{\alpha x,Rk}$	Characteristic axial withdrawal capacity of the fastener (N/mm^2)
$f_{h,0,k}$	Characteristic embedment strength in timber member (N/mm^2)
ρ_k	Characteristic wood density
$F_{v,Rd}$	Design value of resistance per shear plane and per fastener (N)
N	Number of connectors (-)
a_1	Spacing of dowels within one row parallel to the grain (mm)
a_2	Perpendicular to the grain and between rows (mm)

$a_{3,t}$	Distance between fasteners and loaded end (mm)
a_4, c	Distance between fasteners and unloaded edge (mm)
d	Connector diameter (mm)
$E_{d,fi}$	Action design effect for an exposure fire (N/mm^2)
η_f	Conversion factor for slip modulus (-)
$f_{d,fi}$	Design strength in fire (N/mm^2)
$k_{mod,fi}$	Modification factor for fire (-)
$\gamma_{M,fi}$	Partial factor for timber (-)
$t_{d,fi}$	Time of the fire resistance according to the connector (s)
a_{fi}	Thickness of the member for improved a fire resistance (mm)
β_n	Design charring rate under fire exposure (-)
k_{flux}	Heat flux coefficient for fasteners (-)
t_{req}	Required time of fire resistance (s)
t_{ch}	Delay of the start of charring rate due to protection (s)
h_p	Fire protective panel thickness (mm)
β_0	One-dimensional design charring rate under standard fire exposure (-)

FIGURES INDEX

FIGURE 1 - SINGLE-SHEAR TIMBER CONNECTIONS: A) WOOD-WOOD CONNECTION B) WOOD-STEEL CONNECTION [6] 29
FIGURE 2 - DOUBLE-SHEAR TIMBER CONNECTIONS: A) W-W-W CONNECTION B) W-S-W CONNECTION C) S-W-S CONNECTION [6] 29
FIGURE 3 – EXAMPLES OF TRADITIONAL JOINTS [16] 32
FIGURE 4 – A) STRUCTURAL FINGER JOINTS (VERTICAL AND HORIZONTAL) B) SCARF JOINT [16, 18] 33
FIGURE 5 - REPRESENTATION OF A GLUED TYPE CONNECTION [17] 33
FIGURE 6 – EXAMPLES OF BEARING TYPE FASTENERS A) SPLIT-RING CONNECTOR; B) PRESSED STEEL SHEAR PLATE; C) MALLEABLE IRON SHEAR PLATE; D) TOOTHED RING CONNECTOR [19] 34
FIGURE 7 - THREE PRINCIPAL AXES OF WOOD WITH RESPECT TO GRAIN DIRECTION AND GROWTH RINGS [2] 37
FIGURE 8 - WOOD THERMAL CONDUCTIVITY FUNCTION OF THE TEMPERATURE [W/M.K][21] 39
FIGURE 9 - WOOD SPECIFIC HEAT FUNCTION OF THE TEMPERATURE [J/KGK] [21] 40
FIGURE 10 – WOOD DENSITY (GL20H, GL24H, GL32H) FUNCTION OF THE TEMPERATURE [kG/m^3] 42
FIGURE 11 - STEEL THERMAL CONDUCTIVITY FUNCTION OF THE TEMPERATURE [W/mK] [23] 44
FIGURE 12 - STEEL SPECIFIC HEAT FUNCTION OF THE TEMPERATURE [kJ/kGK] [23] 45
FIGURE 13 - GYPSUM TYPE A AND F THERMAL CONDUCTIVITY FUNCTION OF THE TEMPERATURE [W/mK] [24] 46
FIGURE 14 - GYPSUM TYPE A AND F SPECIFIC HEAT FUNCTION OF THE TEMPERATURE [kJ/kGK] [24] 47
FIGURE 15 – GYPSUM TYPE A AND F DENSITY FUNCTION OF THE TEMPERATURE [kG/m^3] [26] 47
FIGURE 16 - DOWEL ARRANGEMENT ACCORDING TO EUROCODE 5, PART 1-1 [28] 53
FIGURE 17 - W-S-W CONNECTION IN STUDY 53
FIGURE 18 - CROSS-SECTIONS USED IN THE NUMERICAL CALCULATION 69
FIGURE 19 – FINITE ELEMENT *PLANE77* GEOMETRY [35] 69
FIGURE 20 - RELATIONSHIP BETWEEN THE APPLIED LOAD (KN) AND THE NUMBER OF DOWELS 73
FIGURE 21 - REPRESENTATION OF THE STUDIED POINTS IN THE MESH MODEL 75
FIGURE 22 – TIME-TEMPERATURE HISTORY DURING 60 MINUTES, MEASURED FOR THE EXTERNAL AND INTERNAL POINTS OF AN UNPROTECTED CONNECTION 76
FIGURE 23 - TEMPERATURE DEVELOPMENT AT TWO DIFFERENT FIR TIME INSTANTS (15 AND 30 MIN) IN THE UNPROTECTED CONNECTION INCLUDED ALL THREE WOOD DENSITIES 77
FIGURE 24 - TEMPERATURE DEVELOPMENT AT 60 MINUTES IN THE PROTECTED CONNECTION USING GYPSUM TYPE A AND F 78
FIGURE 25 - TEMPERATURE PROGRESSION OVER TIME OF 60 MINUTES FOR THE EXTERNAL AND INTERNAL POINTS 79
FIGURE 26 – COMPARISON BETWEEN GYPSUM TYPE A AND F FOR THE EXTERNAL POINTS 80
FIGURE 27 - COMPARISON BETWEEN GYPSUM TYPE A AND F FOR THE INTERNAL POINTS 80
FIGURE 28 - COMPARISON BETWEEN THE UNPROTECTED AND PROTECTED CONNECTIONS FOR THE EXTERNAL POINTS 81
FIGURE 29 - COMPARISON BETWEEN THE UNPROTECTED AND PROTECTED CONNECTIONS FOR THE INTERNAL POINTS 81

TABLES INDEX

TABLE 1 - CHARACTERISTIC STRENGTH AND STIFFNESS PROPERTIES (IN N/mm^2) FOR HOMOGENEOUS GLUED LAMINATED TIMBER [20] 38
TABLE 2 - ELASTIC RATIOS FOR VARIOUS SPECIES AT APPROXIMATELY 12% MOISTURE CONTENT [2] 38
TABLE 3 - POISSON'S RATIOS FOR VARIOUS SOFTWOOD SPECIES AT APPROXIMATELY 12% MOISTURE CONTENT [2] 38
TABLE 4 - WOOD THERMAL CONDUCTIVITY FUNCTION OF THE TEMPERATURE [W/m.K] [21] 39
TABLE 5 - WOOD SPECIFIC HEAT FUNCTION OF THE TEMPERATURE [J/kGK] [21] 40
TABLE 6 - WOOD DENSITY COEFFICIENT FUNCTION OF THE TEMPERATURE [21] 41
TABLE 7 - WOOD DENSITY (GL20H, GL24H, GL32H) FUNCTION OF THE TEMPERATURE, [kG/m^3] 42
TABLE 8 - STEEL MECHANICAL PROPERTIES ACCORDING TO EUROCODE 3, PART 1-1 [22] 43
TABLE 9 – SPACING AND EDGE AND END DISTANCES BETWEEN THE DOWELLED CONNECTIONS [28] 54
TABLE 10 - CONNECTION'S DIMENSIONS FOR THE MECHANICAL DESIGN 74
TABLE 11 - CHARRING RATE FOR THE POINTS IN CONSIDERATION BASED ON THE TYPE OF WOOD [MM/MIN] 75

INDEX

1 INTRODUCTION 23

1.1 Context 23

1.2 Objectives 24

1.3 Dissertation structure 24

2 STATE OF THE ART 29

3 MATERIAL PROPERTIES 37

3.1 Wood 37

3.1.1 Mechanical Properties 37

3.1.2 Thermal Properties 39

3.2 Steel 43

3.2.1 Mechanical Properties 43

3.2.2 Thermal Properties 43

3.3 Gypsum 45

3.3.1 Thermal Properties 46

4 DESIGN OF W-S-W CONNECTION AT ROOM TEMPERATURE 51

4.1 Procedure 51

5 DESIGN OF W-S-W CONNECTION AT HIGH TEMPERATURES 57

5.1 Procedure 57

5.1.1 Unprotect connections 58

5.1.2 Protected connections 58

6 THERMAL ANALYSIS 63

6.1 Modes of Heat Transfer 63

6.1.1 Conduction 63

6.1.2 Convection 64

6.1.3 Radiation 64

6.2 Fire curve 65

6.3 Numerical Thermal Analysis 65

6.3.1 Equations and boundary conditions for heat transfer 65

6.3.2 Finite Element Method 66

6.3.3 Geometry 69

6.3.4 Material Properties 69

6.3.5 Mesh and Element Type 69

7 RESULTS AND DISCUSSION 73

7.1 Mechanical Design 73

7.2 Thermal Analysis 74

7.2.1 Unprotected connections 74

7.2.2 Protected Connections 78

8 CONCLUSIONS AND FUTURE WORK 85

8.1 CONCLUSIONS 85

8.2 FUTURE WORK 86

9 REFERENCES 89

10 ANNEXES 95

10.1 ANNEX 1 95

10.2 ANNEX 2 96

10.3 ANNEX 3 97

10.4 ANNEX 4 103

10.5 ANNEX 5 104

10.6 ANNEX 6 105

10.7 ANNEX 7 108

INTRODUCTION

1 INTRODUCTION

1.1 Context

Throughout the humanity history, the use of wood has been quite extensive and diversified, due to the fact that it is a material with a vast availability, light and easy to handle. With this, it was possible to acquire good knowledge about the characteristics of wood and the behavior of structures, thus allowing the wood to be one of the dominant structural materials in the buildings construction for several centuries [1].

All wood consists of cellulose, hemicelluloses, lignin, and minor amounts (from 5% up to 10%) of extraneous materials incorporated in a cellular structure. The cellular structure, which presents differences according to the volume and characteristics of these components make woods heavy or light, stiff or flexible, and hard or soft. With that said, the properties of a single species are relatively constant within its limits. Thus, the selection of wood by species might sometimes be suitable [2].

There are many factors that keep wood in the forefront of raw materials. However, the major attribute is its availability in many species, shapes, sizes that can fulfill almost every demand. Wood presents a high ratio of strength to weight and a significant record for performance and durability as a structural material. Particularly, dry wood exhibits some great characteristics, such as insulating properties against heat, sound, and electricity. Moreover, it tends to absorb and dissipate vibrations under several use conditions, and it is easily shaped with tools and fastened with different types of connectors. Beyond that, wood resists oxidation, salt water, and other corrosive agents, can be treated with preservatives and fire retardants, and, furthermore, can be combined with almost any other material for both functional and aesthetic uses [2].

In timber constructions, the connections are considered the critical points due to their strength and durability being directly dependent on the type of connection and the different connecting elements used in them. These regions are also subject to localized stresses and strains, which may compromise the overall stability of the structure [3].

In the case of dowel-type connectors, the transmission of forces is ensured by pressure between the connector and the wood on the face of the insertion hole. Its resistance is conditioned by the crushing of the wood in the contact area, possibly associated with the plastification of the connector, which is subject to shear and bending forces [3].

In a fire situation, the constituent elements of a connection have their thermal and mechanical properties altered, which can cause instability of the connection and, therefore, of the whole structure involved [4].

When the wood starts burning, a char layer begins on the surface of the material. This layer allows the insulation of the wood inside, thus protecting it from the external fire action. In this way, wood constructions maintain a substantial part of their resistant capacity when exposed to fire [4]. However, the steel elements used in the connection have a negative effect in this scenario, due to the fact that the heat is conducted inside of the connection. This phenomenon leads to an increase of the char layer and a reduction of the resistant capacity of the connection [5].

1.2 Objectives

The main purposes of the current work are:

- Design of a W-S-W (wood – steel – wood) connection at ambient and high temperature using an analytical methodology based on Eurocode 5;
- Evaluate the thermal behavior of the W-S-W connection when exposed to fire using a numerical methodology based on the finite element method;
- Compare the results obtained with both analytical and numerical methodologies;
- Analyze thermal behavior due to the effect of different wood densities and dowel diameters;
- Evaluate and compare the effect of using different gypsum plasterboards as an insulation material in the connection;

1.3 Dissertation structure

This dissertation is structured in eight chapters: 1 - *Introduction*, 2 - *Bibliographic work*, 3 - *Material properties*, 4 - *Design of W-S-W connection at ambient temperature*, 5 - *Design of W-S-W connection at high temperature*, 6 - *Thermal analysis*, 7 - *Results and discussion* and 8 - C*onclusions and future developments*.

Subsequent to the current chapter, comes *Chapter 2 – Bibliographic work,* where are introduced some relevant researches and scientific works that were used as a groundwork for the current master thesis.

In *Chapter 3 – Material properties,* are presented the main thermal properties (thermal conductivity, specific heat, and density) for all the used materials (wood, steel, and gypsum) required in the thermal analysis implemented in this research.

In *Chapter 4 - Design of W-S-W connection at ambient temperature*, is presented the calculation method stated in Eurocode 5 used in the design of the generic model of a W-S-W connection.

In *Chapter 5 - Design of W-S-W connection at high temperature,* is presented the calculation method detailed in Eurocode 5 *under fire exposure* used in the design of the generic model of a W-S-W connection.

In *Chapter 6 – Thermal analysis,* is presented with all the required data for the development of the thermal analysis. In the first instance, a brief introduction of the heat transfer modes (conduction, convection, and radiation), the used fire curve, and the finite element method (FEM) is presented. Afterward, the numerical model of the W-S-W connection and its specifications implemented in the simulation are presented.

In *Chapter 7 – Results and discussion,* it is present and discussed all the obtained results in all the carried out numerical simulations and, then compared with the analytical results.

In *Chapter 8 – Conclusions and future developments* contain the main conclusions of this work, as well as some future work proposals.

STATE OF THE ART

2 STATE OF THE ART

Wood connections are the subject of studies by many researchers in various countries, it is considered one of the essential parts of a timber structure and therefore requires more considerable attention during the design. These connections are so meaningful because these are always the weakest parts of the structure. However, they govern the load-carrying capacity of the structure. Thus, the resistance and the durability of these types of structures are mainly dependent on the joints design between the elements [6].

According to Eurocode 5 part 1-1, the design of wood connections is emphasized more than timber members, such as beams and columns, to ensure the stability of the structure. Depending on which application, the connection has different options for the fasteners, as represented in figures 1 and 2, using bolts or dowels, and steel plates more prevalent on massive timber structures, since they are able to carry heavy loads [6].

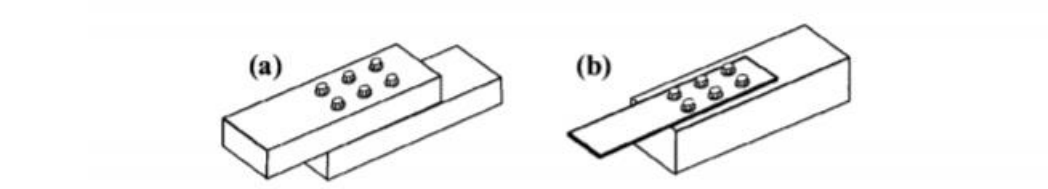

Figure 1 - Single-shear timber connections: a) wood-wood connection b) wood-steel connection [6]

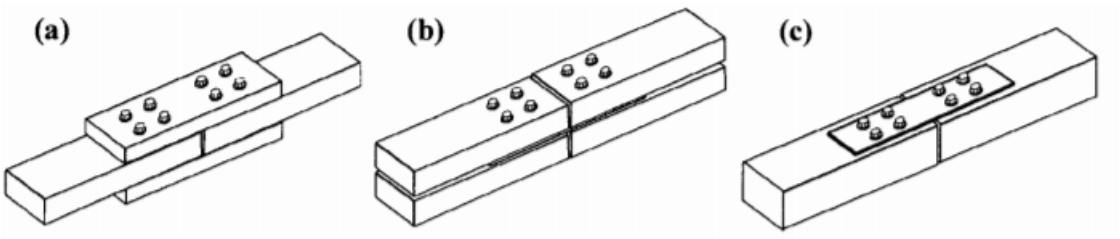

Figure 2 - Double-shear timber connections: a) W-W-W connection b) W-S-W connection c) S-W-S connection [6]

Under fire exposure, due to the heat being conducted deep into the wood members by the metal fasteners causing faster wood charring, makes it necessary for an in-depth thermal analysis. The capacity of these connections under fire exposure depends on the wood charring rate and the strength reduction of the metal fasteners as well as the wood residual cross-section [7].

The determination of the load-carrying capacity and thermal resistance is a very complicated task, due to the high number of parameters under study, such as various connection types, different fastener arrangements, the wood properties variability and the char-layer formation at elevated temperatures.

Johansen was the first who described the mechanical behavior of these types of connections. His theory characterizes three distinct failure modes. However, his theory does not consider potential brittle failure modes. By introducing some changes and adaptions, Johansen's theory is the foundation for the so-called European Yield Model, which is currently used in the design codes (Eurocode 1995-EC5) for timber structures [8].

At least since the late 1970s and early 80s, fire tests on timber connections were conducted, particularly in Germany, Denmark, Sweden, and Finland [9].

EN 1995-1-2:2004 is based on a test that was performed in the late 1990s by Norén (1996), Dhima (1999), as well as by Kruppa, Lamadon, and Racher (2000). These tests were based on splice connections loaded in tension, particularly three-member wood-to-wood and steel-to-wood connections (with an internal steel plate) exposed to fire on all sides [9].

In 2013, C. Maraveas worked with wood connections exposed to fire and verified the performance of connections design and, therefore, established the overall fire resistance of the structure, concluding about the zones that are commonly the weakest ones in timber constructions. Both numerical and experimental studies on the fire resistance of the regular components, such as wood-wood-wood (W-W-W), wood-steel-wood (W-S-W) and steel-wood-steel (S-W-S) connections were introduced and, thus, the effect of some parameters was studied. The results of this study reveal that wood connections are extremely vulnerable to fire exposure. The unprotected joints loaded axially have the fire rating is generally less than 30 min. Therefore, the application of fire protection is the most effective solution [10].

In 2009, A. Frangi, C. Erchinger, and M. Fontana made several fire tests in order to analyze two types of steel-to-wood connections. Thus, they found out that the unprotected multiple shear steel-to-wood connections with dowels designed for ambient temperature achieve a fire resistance of around 30 min. By increasing the end distance of the dowels by 40 mm as well as the side wood member, the connection reaches a fire resistance of more than 70 min. Beyond that, the unprotected connections with steel side plates and annular ring nails failed after around 12 min accompanied by a significant deformation of the nails. On the other hand, by using the

intumescent paint as protection for the steel side plates, the fire resistance of the connection can raise to 30 min [11].

In 2010, Lei Peng et al. considered that there are calculation models developed in the prediction of the fire resistance of double-shear wood connections. In order to analyze heat transfer within bolted wood-wood-wood (W-W-W), wood-steel-wood (W-S-W) and steel-wood-steel (S-W-S) connections, a three-dimensional finite-element thermal model was used. Comparing with experimental results, the obtained results with the current calculation model revealed that the method might fairly forecast the fire resistance of W-W-W and W-S-W connections with an accuracy of around ± 15%. However, for S-W-S connections, this accuracy reaches values of around ± 10%. Additionally, this method may be modified by introducing safety factors in order to ensure the prediction on the conservative side [6].

In 2016, the author conducted experimental tests with the purpose of determining the behavior of connections with a connector, thus studying the influence of different connectors diameters, wood thickness of the wood element, and load angle in relation to the orientation of the wood grain. It was possible to verify that increasing the thickness of the wood element increases the strength of the connection. In relation to the angle between the load and the grain, a strong influence between both variables was verified [12].

In 2013, M. Audebert et al. worked out a three-dimensional numerical model that allows the simulation of the thermo-mechanical behavior of bolted and dowelled wood-to-wood connections loaded in tension parallel to the grain. The comparison between the experimental and the numerical method using nonlinear load-displacement curves shows that numerical modeling provides satisfactory results respecting to the global nonlinear behavior of the connections. Nevertheless, the comparison under fire exposure exhibits a similar tendency. The fire resistance times reached with the numerical model are always shorter in comparison with those observed experimentally, reaching an average relative deviation of around 33% [13].

Simon Schnabl worked with mathematical models based on partial differential equations, which determined the charring rate and temperature gradients for combined heat and moisture transfer in wood beams. The results of his research showed a good agreement between the developed model and the results presented in the literature [14].

In 2009 a comparison of four different gypsum plasterboards available on the European market was carried out. The comparison between their thermal properties when exposed to fire conditions imposed by the ISO834 curve was evaluated. The

present comparison was made by invoking not only experimental methods, but also 2D numerical simulations in the software VOLTRA. The experimental results show the importance of calcium sulfate, calcium carbonate as well as magnesium carbonate percentages included in the gypsum plasterboard composition. With respect to the numerical simulation results, it was proved that the percentage of calcium sulfate is essential to the gypsum's response to the fire during the first 30 minutes [15].

This research will be focused on the wood-steel-wood (W-S-W) connection type with dowels as the connector, therefore, it is presented a mechanical connection. That being said, there are three types of connections, the carpentry joints, the bonded connections, and the mechanical connections.

The carpentry joints (traditional) are connected timber elements, usually subjected to compressive axial loads, relying on these compression internal forces to keep facing surfaces in close contact, often without any other devices but notches in the connected members, as represented in figure 3. The carpenter connections are not included in Eurocode 5 and only national regulations are applied [3].

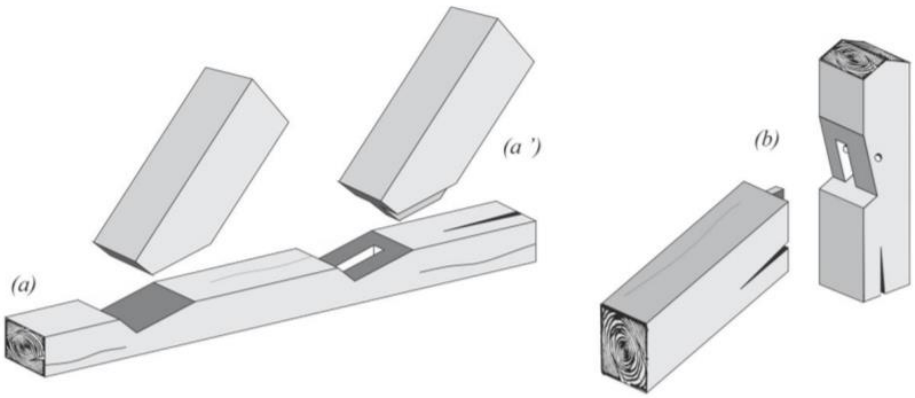

Figure 3 – Examples of traditional joints [16]

The bonded connections are usually employed to connect new and reinforce existing members in timber structures. There are several types of bonded connections, such as structural finger joints (figure 4) and glued-in steel rods (figure 5). This type of glued connections follows national regulations in design construction. This type of connections provides a higher fire rating as well as more aesthetically look in comparison with the dowel-type connections due to the inclusion of steel rods inside the timber member, as exemplified in figure 5 [17].

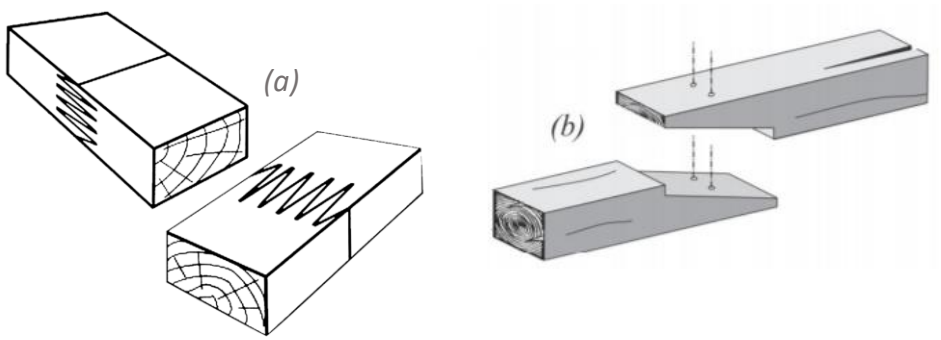

Figure 4 – a) structural finger joints (vertical and horizontal) b) scarf joint [16, 18]

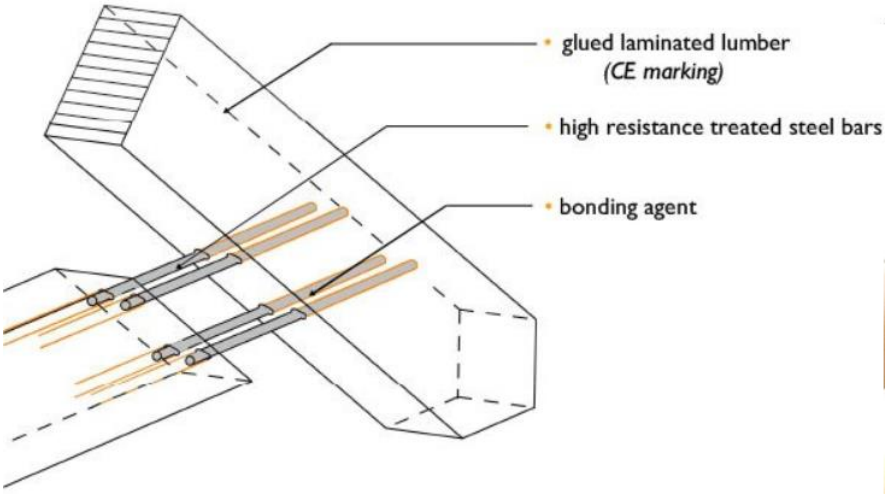

Figure 5 - Representation of a glued type connection [17]

Mechanical connections are divided between dowel type fasteners and bearing type connections. Dowel type fasteners, represented in figure 6, such as bolts, screws, and nails, transmit either lateral or withdrawal loads. Lateral loads are transmitted by bearing stresses developed between the fastener and the members of the connection, and the withdrawal loads are axial loads parallel to the fastener axis transmitted through friction or bearing to the connected materials. Metal connector plates are a particular case of dowel type fasteners since they combine the lateral load actions of dowel fasteners and the strength properties of the metal plates [2, 3].

Unlike the dowel type fasteners, bearing type fasteners transmit lateral loads only. Bearing type fasteners, represented in figure 6, such as split-ring connectors and shear plates, transmit shear forces through bearing on the connected materials. Hanger-type connections are a combination of dowel and bearing-type fasteners where, generally, support one structural member and are connected to another member by a combination of dowel and bearing action [2, 3].

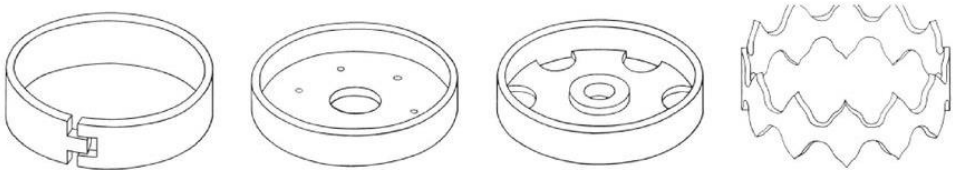

Figure 6 – Examples of bearing type fasteners a) split-ring connector; b) Pressed steel shear plate; c) Malleable Iron shear plate; d) Toothed ring connector [19]

The selection of a fastener for a specific design application depends on the type of connection and the required strength capacity. Each connection must be designed to transmit forces effectively and provide acceptable performance for the life of the structure without causing cracking, splitting, or excessive deformation of the elements. The strength of mechanical fasteners is dependent on many factors, such as lumber species (density or specific gravity), angle of load to grain, the spacing of mechanical fasteners, and edge and end distances [2, 3].

MATERIAL PROPERTIES

3 MATERIAL PROPERTIES

In the case of structural analysis, it is essential to know the properties of the materials present in the connection. In this chapter the mechanical and thermal properties of the wood, steel, and gypsum, are exhibit both used in this work.

3.1 Wood

3.1.1 Mechanical Properties

Wood may be described as an orthotropic material, in other words, it has unique and independent mechanical properties in the directions of three mutually perpendicular axes: longitudinal, radial, and tangential, as pictured in figure 7. The longitudinal axis L is parallel to the fiber (grain), the radial axis R is normal to the growth rings (perpendicular to the grain in the radial direction), the tangential axis T is perpendicular to the grain but tangent to the growth rings [2].

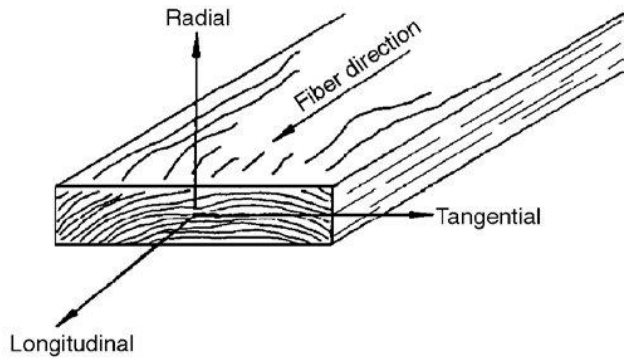

Figure 7 - Three principal axes of wood with respect to grain direction and growth rings [2]

3.1.1.1 Glued Laminated Timber

In the present work, will be used three types of glued laminated wood (GL20H, GL24H, and GL32H) which is commonly applied in construction engineering.

The designation GL refers to the fact that it is a laminated glued wood; the following number defines its resistance to bending, and finally, the last letter, H or C, distinguishes the type of beam, homogeneous or combined, respectively. The mechanical properties for this type of wood can be consulted in Table 1 [20].

Table 1 - Characteristic strength and stiffness properties (in N/mm^2) for homogeneous glued laminated timber [20]

Strength class (N/mm^2)		GL20H	GL24H	GL32H
Bending strength	$f_{m,g,k}$	20	24	32
Tensile strength	$f_{t,0,g,k}$	16	19,2	25,6
	$f_{t,90,g,k}$	0,5		
Compressive strength	$f_{c,0,g,k}$	20	24	32
	$f_{c,90,g,k}$	2,5		
Shear strength	$f_{v,g,k}$	3,5		
Modulus of elasticity	$E_{0,g,mean}$	8400	11500	14200
	$E_{0,g,05}$	7000	9600	11800
	$E_{90,g,mean}$	300		
	$E_{90,g,05}$	250		
Shear modulus	$G_{g,mean}$	650		
	$G_{g,05}$	540		

Due to its properties, the glued laminated wood used in the study can be compared to the wood coming from a Spruce, Sitka. Tables 2 and 3 show the elastic properties of this type of wood. It is essential to remember that wood is an orthotropic material and therefore its properties vary according to the directions mentioned above [2].

Table 2 - Elastic ratios for various species at approximately 12% moisture content [2]

Species	E_T/E_L	E_R/E_L	G_{LR}/E_L	G_{LT}/E_L	G_{RT}/E_L
Spruce, Sitka	0,372	0,467	0,435	0,245	0,040

Table 3 - Poisson's ratios for various softwood species at approximately 12% moisture content [2]

Species	μ_{LR}	μ_{LT}	μ_{RT}	μ_{TR}	μ_{RL}	μ_{TL}
Spruce, Sitka	0,372	0,467	0,435	0,245	0,040	0,025

3.1.2 Thermal Properties

Thermal properties explain the response of a material to the application of heat, being some of them essential to steady thermal analysis and others essential to unsteady thermal conditions, such as the fire.

3.1.2.1 Thermal Conductivity

Thermal conductivity is a measure of the heat flow rate through one unit thickness of a material subjected to a temperature gradient. The wood conductivity values are shown in table 4. Figure 8 shows the variation of thermal conductivity with temperature as referred to in Eurocode 5, part 1-2 for design purposes [21].

Table 4 - Wood thermal Conductivity function of the temperature [W/m.K] [21]

Temperature [°C]	Thermal Conductivity [W/m.K]
20	0,12
200	0,15
350	0,07
500	0,09
800	0,35
1200	1,5

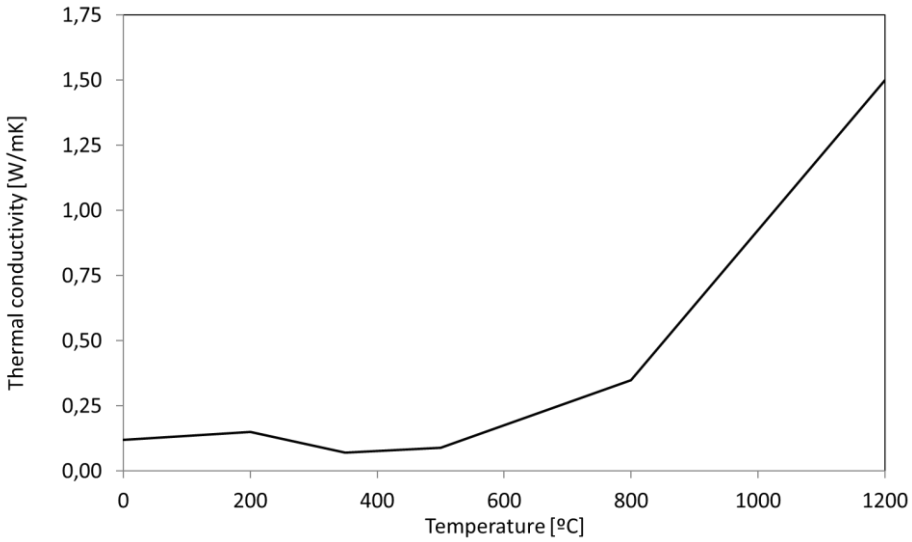

Figure 8 - Wood Thermal Conductivity function of the temperature [W/m.K][21]

3.1.2.2 Specific Heat

The specific heat is defined as the amount of heat required for a single unit of mass to be raised by one degree of temperature. The specific heat of wood depends on various factors such as the temperature and moisture content of the wood. However, it is practically independent of material density or species [2].

The values of the specific heat are presented in table 5 and figure 9, as referred to on Eurocode 5, part 1-2 [21].

Table 5 - Wood Specific Heat function of the temperature [J/kgK] [21]

Temperature [°C]	Specific heat, J/kg.K
0	1530
99	1770
110	13600
120	13500
130	2120
200	2000
250	1620
300	710
350	850
400	1000
600	1400
800	1650
1200	1650

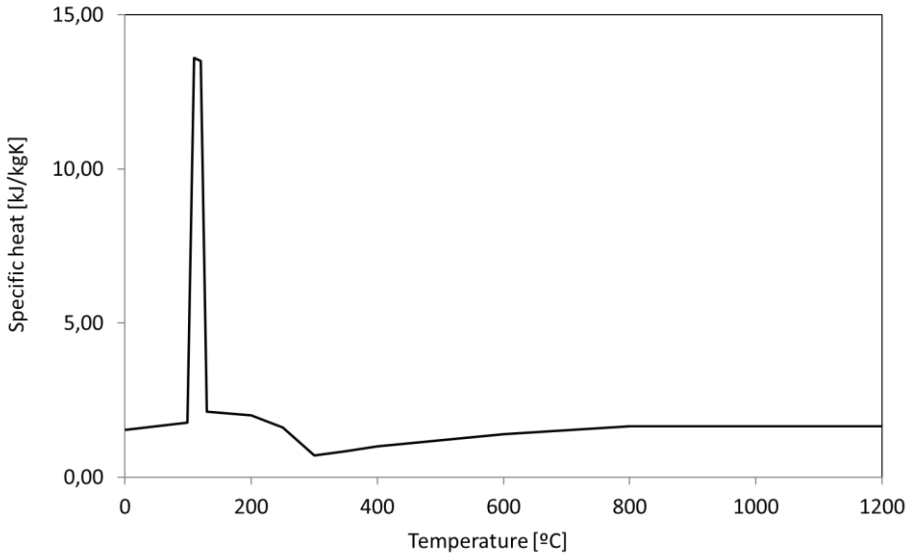

Figure 9 - Wood Specific Heat function of the temperature [J/KgK] [21]

3.1.2.3 Density

Wood is used in a wide range of conditions and has a wide range of moisture content values in use. Because of the fact that moisture makes up part of the global weight of the product, the wood density is being determined and reported based on moisture content in use [2].

The value of the wood density is often based on average species characteristics. Therefore, this value should be considered as an approximation due to the natural variation in anatomy, moisture content, and the ratio of heartwood to sapwood that exists. Although, this value of density is decently accurate to allow the suitable application of wood as a structural material [2].

The wood density coefficient, shown in table 6, correspond to a moisture content average of 12% (ω) as referred to on Eurocode 5, part 1-2 [21].

Table 6 - Wood Density Coefficient function of the temperature [21]

Temperature (ºC)	Density Coefficient
0	1 + ω
99	1 + ω
120	1
200	1
250	0,93
300	0,76
350	0,52
400	0,38
600	0,28
800	0,26
1200	0

The variation of density of the three types of wood (GL20H, GL24H, GL32H) with temperature is shown in table 7 and depicted in figure 10. The represented values of the density coefficient for each temperature were obtained according to table 6 considering the density value of 370, 400, and 480 kg/m^3, respectively, for the wood type GL20H, GL24H, and GL32H.

Table 7 - Wood density (GL20H, GL24H, GL32H) function of the temperature, [kg/m^3]

Temperature (ºC)	Density Coefficient		
	GL20H	GL24H	GL32H
0	414,4	448	537,6
99	414,4	448	537,6
120	370	400	480
200	370	400	480
250	344,1	372	446,4
300	281,2	304	364,8
350	192,4	208	249,6
400	140,6	152	182,4
600	103,6	112	134,4
800	96,2	104	124,8
1200	0	0	0

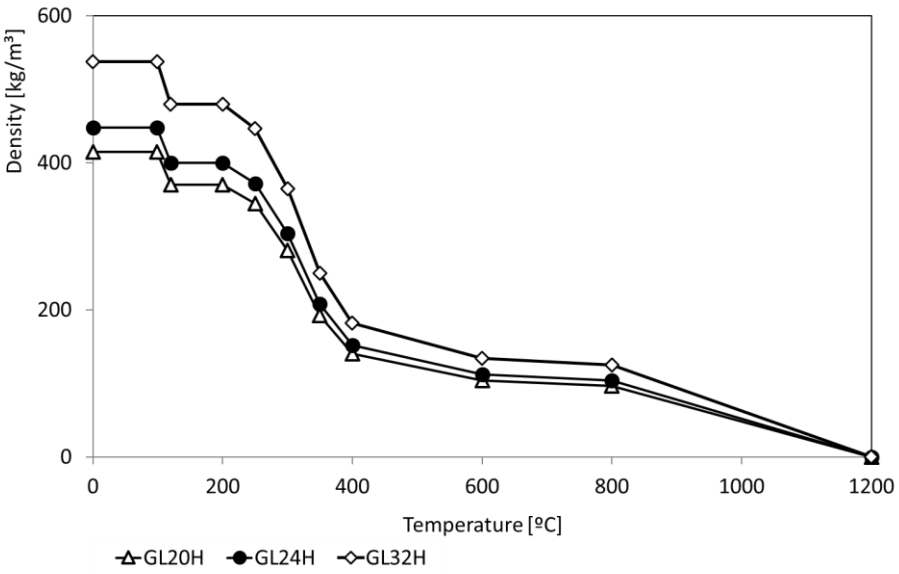

Figure 10 – Wood density (GL20H, GL24H, GL32H) function of the temperature [kg/m^3]

3.2 Steel

3.2.1 Mechanical Properties

The material coefficients and the elastic constants used at ambient temperature to be adopted in calculations for the steel design parts of this work should be taken as shown in table 8, as referred in Eurocode 3, part 1-1 [22].

Table 8 - Steel mechanical properties according to Eurocode 3, part 1-1 [22]

Modulus of elasticity (E)	$210000\ MPa$
Shear modulus (G)	$\frac{E}{2(1+\nu)} = 81000\ MPa$
Poisson's ration in elastic stage	0,3
Coefficient of linear thermal expansion	$12 \times 10^{-6}\ [K^{-1}]\ (T \leq 100\ ^{o}C)$

3.2.2 Thermal Properties

According to Eurocode 3, part 1-2, there are several equations for the calculation of the thermal properties of the steel [23].

The density of steel remains constant with temperature, equal to 7850 kg/m^3. The emissivity of the material was considered equal to 0.7 [23].

3.2.2.1 Thermal Conductivity

The thermal conductivity of steel λ_a should be determined from equations 1 and 2 [23].

For $20^oC \leq \theta_\alpha \leq 800^oC$:

$$\lambda_a = 54 - 3{,}33 \times 10^{-2}\ \theta_a \quad \left[\frac{W}{m.K}\right] \tag{1}$$

For $800^oC \leq \theta_\alpha \leq 1200^oC$:

$$\lambda_a = 27{,}3 \quad \left[\frac{W}{m.K}\right] \tag{2}$$

Where θ_α is the steel temperature [^{o}C]

The variation of the thermal conductivity with temperature can be illustrated in figure 11 [23].

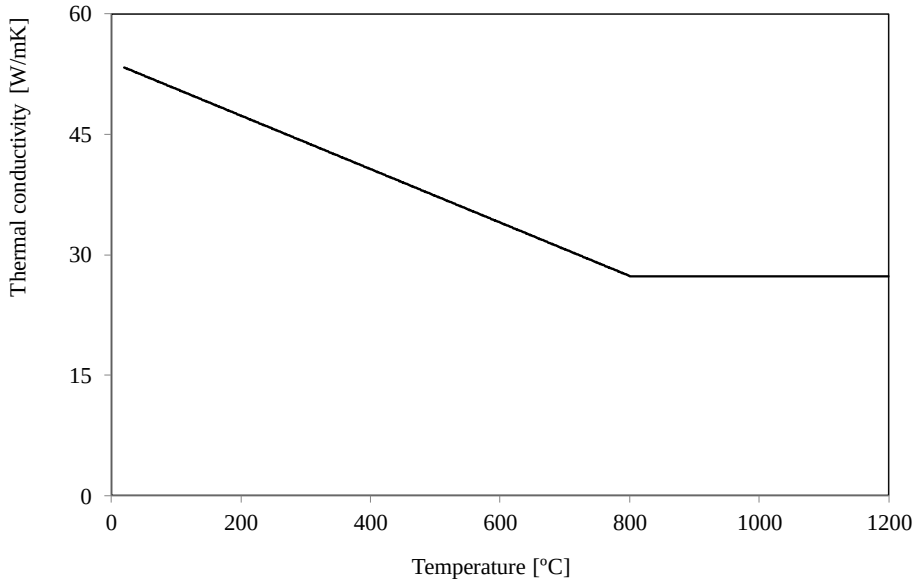

Figure 11 - Steel Thermal Conductivity function of the temperature [W/mK] [23]

3.2.2.2 Specific Heat

The specific heat of steel C_a should be determined from the following equations [23].

For 20ºC ≤ θ_α ≤ 600ºC:

$$C_a = 425 + 7{,}73 \times 10^{-1}\,\theta_a - 1{,}69 \times 10^{-3}\,\theta_a{}^2 + 2{,}22 \times 10^{-6}\,\theta_a{}^3 \quad \left[\frac{J}{kgK}\right] \qquad (3)$$

For 600ºC ≤ θ_α ≤ 735ºC:

$$C_a = 666 + \frac{13002}{738 - \theta_a} \quad \left[\frac{J}{kgK}\right] \qquad (4)$$

For 735ºC ≤ θ_α ≤ 900ºC:

$$C_a = 545 + \frac{17820}{\theta_a - 731} \quad \left[\frac{J}{kgK}\right] \qquad (5)$$

For 900°C ≤ θ_α ≤ 1200°C:

$$C_a = 650 \ \left[\frac{J}{kgK}\right] \quad (6)$$

Where θ_α is the steel temperature [°C]

The variation of the specific heat with temperature can be displayed in figure 12 [23].

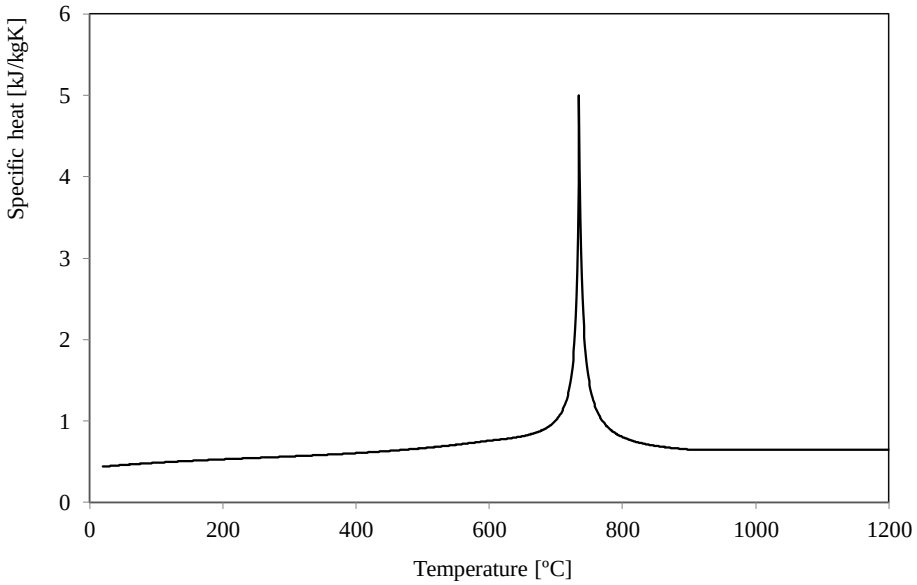

Figure 12 - Steel Specific Heat function of the temperature [kJ/kgK] [23]

3.3 Gypsum

Gypsum plasterboards systems are widely used in buildings, as walls or ceilings, to provide passive fire protection. Opposing to active fire protection procedures, passive fire protection usually means do not need electronic activation or a degree of motion. Passive fire protection remains inactive in the coating system until a fire occurs. In order to accomplish the fire protection and life safety, the structural integrity is maintained for a time during the fire, and limiting the fire spread and its effects [24, 25].

The basis of the fire resistance of gypsum plasterboards lies in low thermal conductivity and the water content evaporation, which absorbs a considerable amount of heat, thereby delaying temperature rise through the system. Thermal properties of gypsum are also temperature-dependent, and among them, thermal conductivity has a critical influence, with a wide range in literature. The variety of thermal properties (density, specific heat, and conductivity) influencing the fire protection ability of different products of gypsum is vast [24, 25].

3.3.1 Thermal Properties

Using the literature, it is possible to find gypsum thermal properties. In this research, it will be used two different types of gypsum plasterboards, the gypsum type A and the type F, one for fire situation and the other for standard applications.

3.3.1.1 Thermal conductivity

The thermal conductivity of gypsum is relatively complex due to the effect of moisture and radiation in the pores. The variation of the thermal conductivity with temperature can be illustrated in figure 13 [24].

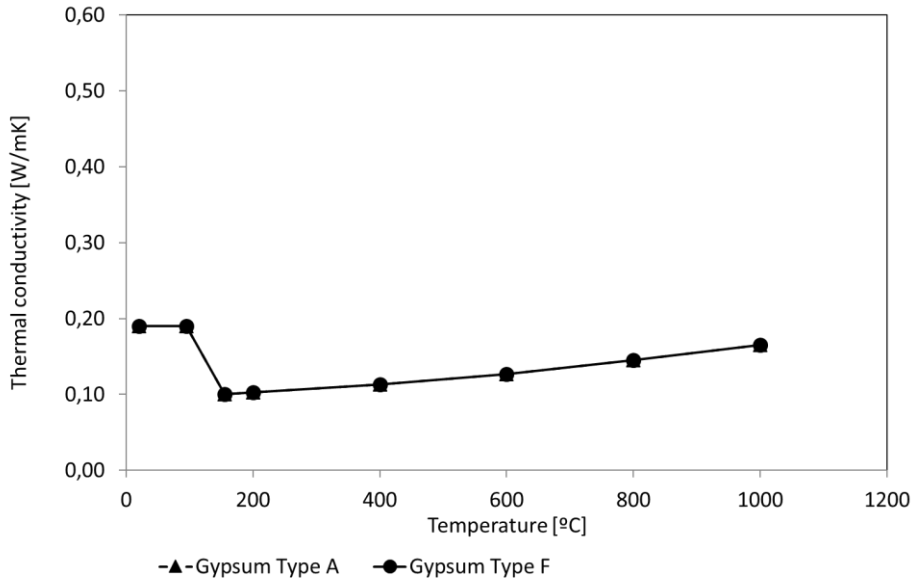

Figure 13 - Gypsum Type A and F Thermal Conductivity function of the temperature [W/mK] [24]

3.3.1.2 Specific Heat

The specific heat taking into account the different chemical reactions during heating presents two peaks. The first peak represents the two endothermic reactions of the gypsum dehydration, and the second peak represents the calcium magnesium carbonate decomposition. The variation of the specific heat with temperature is displayed in figure 14 [24].

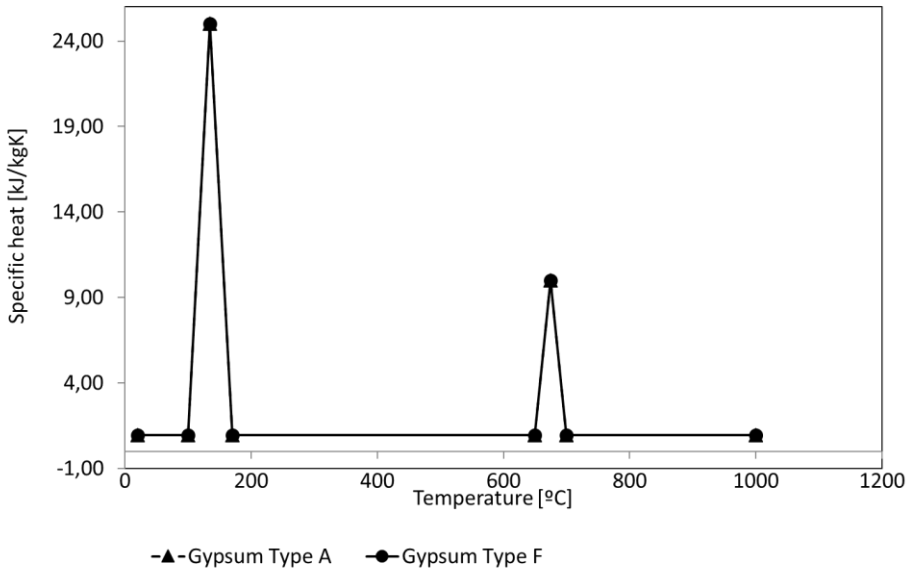

Figure 14 - Gypsum Type A and F Specific Heat function of the temperature [kJ/kgK] [24]

3.3.1.3 Density

The density is affected by the mass loss, which remains almost unchanged up to 100ºC and between 100-160ºC decreases 15-17% as moisture is driven off, and then remains fairly constant. The variation of the density with temperature is displayed in figure 15 for gypsum type A and F [26].

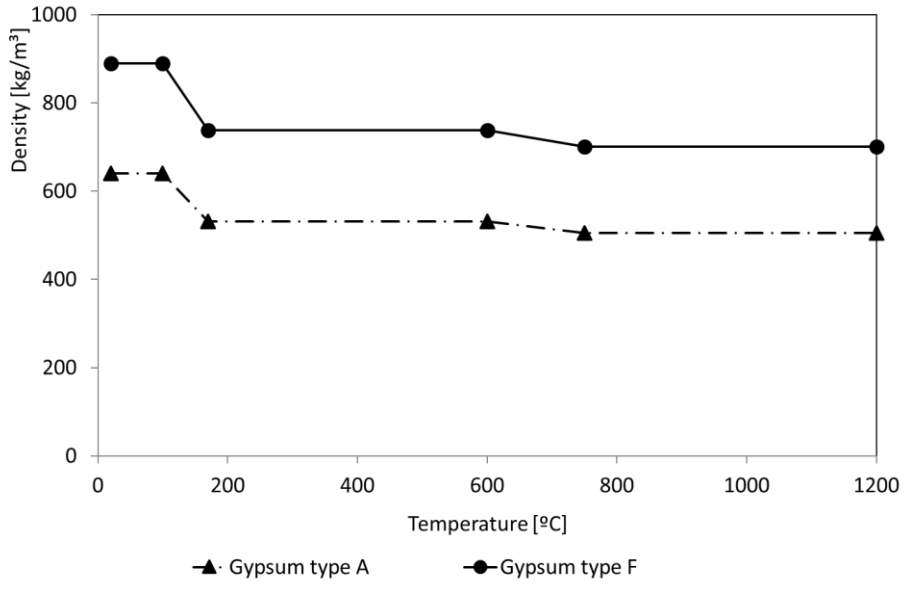

Figure 15 – Gypsum Type A and F Density function of the temperature [kg/m^3] [26]

DESIGN OF W-S-W CONNECTION AT ROOM TEMPERATURE

4 DESIGN OF W-S-W CONNECTION AT ROOM TEMPERATURE

The design of wood connections under double shear intends to determine the main dimensions (width, height, and thickness of the wood plates and steel plate, minimum spacing and edge/end distances between the dowels and the wood plate). The number of dowels is an essential parameter in the design of the connection with the arrangement in lines and columns [27].

During this study, different parameters are considered: tensile applied load E_d, dowel diameters d, the wooden board thickness t_1, t_2 and steel plate thickness t_s. In order to calculate the dimension of the connection, the load was considered as parallel to the grain direction [27].

4.1 Procedure

This procedure was done according to Eurocode 5, part 1-1 [28]. In the first instance, the ultimate limit state must be verified. In case of tension parallel to the grain the following expression shall be satisfied,

$$\sigma_{t,0,d} \leq f_{t,0,d} \tag{7}$$

where $\sigma_{t,0,d}$ is the design tensile stress along the grain and $f_{t,0,d}$ is the design tensile strength along the grain.

The tensile strength, given by the equation 8, represents a reduced value of the characteristic strength along the wood grain, due to the application of two safety factors, one is the modification factor for load duration and moisture content k_{mod}, and the other is the partial factor for material properties γ_M.

$$f_{t,0,d} = \frac{k_{mod}\ x\ f_{t,0,k}}{\gamma_M} \tag{8}$$

On the other hand, the design tensile stress along the grain $\sigma_{t,0,d}$ is calculated using equation 9,

$$\sigma_{t,0,d} = \frac{F_d}{A_s} \tag{9}$$

where F_d is the applied design force and A_s the cross-section of the member.

In these type of connections and for a steel plate of any thickness as the central member of a double shear connection, the characteristic load-carrying capacity per shear plane and per fastener is calculated using the equation 10,

$$F_{v,Rk} = min \begin{cases} f_{h,1,k}\, t_1\, d \left[\sqrt{2 + \dfrac{4 M_{y,Rk}}{f_{h,1,k}\, d\, t_1^2}} - 1 \right] + \dfrac{F_{\alpha x,Rk}}{4} \\ 2{,}3 \sqrt{M_{y,Rk}\, f_{h,1,k}\, d} + \dfrac{F_{\alpha x,Rk}}{4} \end{cases} \quad (10)$$

where, $f_{h,1,k}$ is the characteristic embedment strength in timber member, $M_{y,Rk}$ is the characteristic yield moment of the fastener and $F_{\alpha x,Rk}$ represents the characteristic axial withdrawal capacity of the fastener.

The value of $M_{y,Rk}$ is calculated according to the dowel diameter d, and the material strength of the dowel $f_{u,k}$.

$$M_{y,Rk} = 0{,}3\, f_{u,k}\, d^{2,6} \quad (11)$$

The value of the characteristic embedment strength in timber member $f_{h,0,k}$, is obtained due to the value of the dowel diameter and the characteristic wood density ρ_k.

$$f_{h,0,k} = 0{,}082(1 - 0{,}01d)\rho_k \quad (12)$$

After calculated the value of $F_{v,Rk}$, it is necessary for the application of two safety factors, as shown in Eurocode 5, part 1-1 [28], equation 13.

$$F_{v,Rd} = \frac{F_{v,Rk} \times K_{mod}}{\gamma_M} \quad (13)$$

With the value of $F_{v,Rd}$, it is now possible to obtain the minimum number of the connectors, equation 14.

$$N = \frac{F_d}{F_{v,Rd}} \quad (14)$$

According to Eurocode 5, part 1-1 [28], the dowels arrangement is given by figure 16.

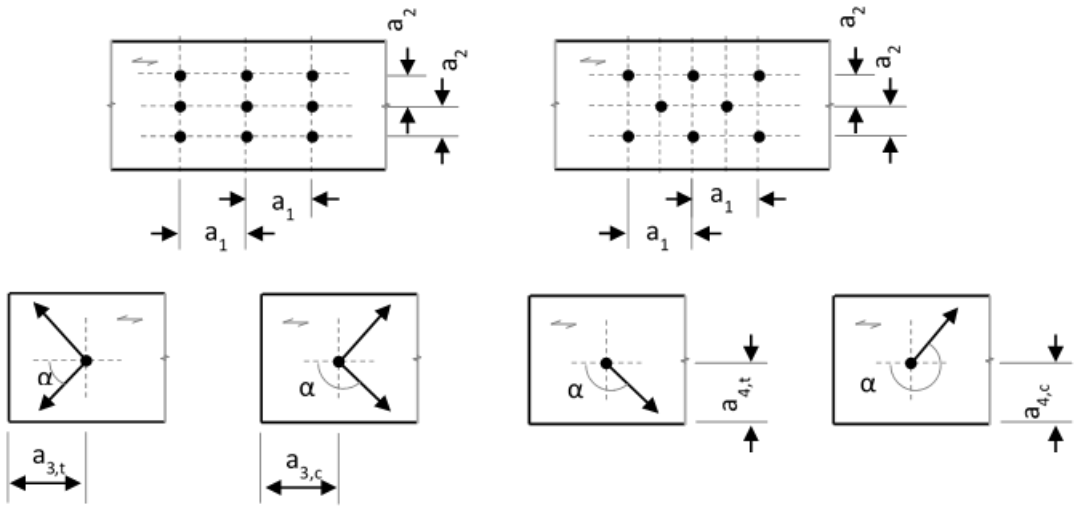

Figure 16 - Dowel arrangement according to Eurocode 5, part 1-1 [28]

In figure 16, a_1 represents the spacing of dowels within one row parallel to the grain, a_2 perpendicular to the grain and between rows, $a_{3,t}$ the distance between fasteners and loaded end, and a_4, c unloaded edge, which varies according to the dowel diameter. Figure 17 represents the model of the connection (W-S-W), considering all variables in study.

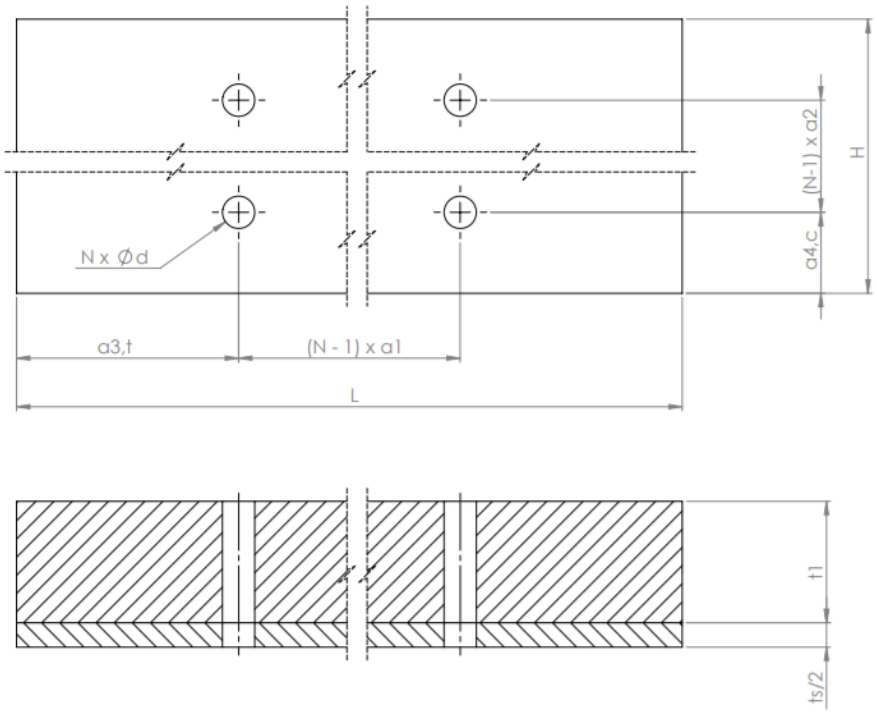

Figure 17 - W-S-W connection in study

The minimum value of spacing and edge and end distances between the dowelled connections are presented in table 9 [28].

Table 9 – Spacing and edge and end distances between the dowelled connections [28]

Spacing and edge/ end distances	Angle	Minimum spacing or edge/ end distance
a_1 (Parallel to grain)	$0° \leq \alpha \leq 360°$	$(3 + 2\lvert\cos\alpha\rvert) \times d$
a_2 (Perpendicular to grain)	$0° \leq \alpha \leq 360°$	$3d$
$a_{3,t}$ (Loaded end)	$-90° \leq \alpha \leq 90°$	$\max(7\ d; 80\ mm)$
$a_{3,c}$ (Unloaded end)	$90° \leq \alpha \leq 150°$ $150° \leq \alpha \leq 210°$ $210° \leq \alpha \leq 270°$	$\max(a_{3,c}\lvert\sin\alpha\rvert) \times d; 3d$ $3d$ $\max(a_{3,c}\lvert\sin\alpha\rvert) \times d; 3d$
$a_{4,t}$ (Loaded edge)	$0° \leq \alpha \leq 180°$	$\max(2 + 2\sin\alpha) \times d; 3d$
$a_{4,c}$ (Unloaded edge)	$180° \leq \alpha \leq 360°$	$3d$

DESIGN OF W-S-W CONNECTION AT HIGH TEMPERATURES

5 DESIGN OF W-S-W CONNECTION AT HIGH TEMPERATURES

Like most building elements, the fire resistance of timber members must be verified. Calculation methods allowance a fast and cheap means of evaluating the load-bearing resistance of timber members. On the other hand, fire tests are expensive and time-consuming [2].

In general, simulations of the fire performance of timber members use effective material properties to include effects such as cracks and degradation of the char layer, as well as the mass flow in the timber member [2].

5.1 Procedure

In Eurocode 5, part 1-2 [21], two different methodologies for safety verification under fire conditions are presented: the simplified method and the reduced load method. In this work, the simplified method will be used in all wood connections.

The following calculations are presented for a fire scenario, according to a time exposure of 30 minutes, for unprotect connections. First, it must be verified if the connection has a fire resistance for the established time, if not, the geometry must be increased in wood cross-section, or adding one type of insulating material to the connection. The action design effect for an exposed fire $E_{d,fi}$ must be calculated. The conversion factor for slip modulus is nominated as η_f.

$$E_{d,fi} = E_d \, \eta_f \tag{15}$$

The design strength in fire $f_{d,fi}$, is calculated using the modification factor for fire $k_{mod,fi}$, and the partial factor for timber $\gamma_{M,fi}$. The value of f_{20} corresponds to the wood strength multiplied by the coefficient k_{fi}, as shown in equation 17.

$$f_{d,fi} = k_{mod,fi} \frac{f_{20}}{\gamma_{M,fi}} \tag{16}$$

$$f_{20} = k_{fi} f_k \tag{17}$$

Using equation 18, it is possible to verify if the connection resists 30 minutes under fire.

$$\frac{E_{d,fi}}{A_s} < f_{d,fi} \quad (18)$$

In case the above equation is not verified, one of two solutions must be chosen: add wood material to the cross-section or add insulating material.

5.1.1 Unprotect connections

For unprotect connection, Eurocode 5, part 1-2 [21] ensures a time of the fire resistance, $t_{d,fi}$, according to the connector. For dowels, this time is 20 minutes, however the minimum value for t_1 is 45mm.

The extra thickness of the member for improved a fire resistance in the connections a_{fi}, is obtained following equation 19.

$$a_{fi} = \beta_n \, k_{flux} \left(t_{req} - t_{d,fi}\right) \quad (19)$$

The β_n value is the design charring rate under fire exposure, k_{flux} is the heat flux coefficient for fasteners, and at last, t_{req} represents the required time of fire resistance.

5.1.2 Protected connections

For connections with an insulating material, the Eurocode 5, part 1-2 [21] gives two options for the material: gypsum (type A, F or H) or wood-based panels. For each one, with different equations are presented. The value t_{ch} refers to the delay of the start of charring rate due to protection, h_p is the fire protective panel thickness, and β_0 is the one-dimensional design charring rate under standard fire exposure.

For wood-based panels:

$$t_{ch} \geq t_{req} - 0{,}5 \, t_{d,fi} \quad (20)$$

$$h_p = t_{ch}\beta_0 \quad (21)$$

For gypsum, type A or H:

$$t_{ch} \geq t_{req} - 0{,}5\ t_{d,fi} \tag{22}$$

$$h_p = \frac{t_{ch} + 14}{2{,}8} \tag{23}$$

For gypsum, type F:

$$t_{ch} \geq t_{req} - 1{,}2\ t_{d,fi} \tag{24}$$

$$h_p = \frac{t_{ch} + 14}{2{,}8} \tag{25}$$

In this research, two different types of gypsum plasterboards will be used, the gypsum type A and the type F, one for standard applications and the other for fire situation, in order to compare and visualize their effects on the protection of the connection.

THERMAL ANALYSIS

6 THERMAL ANALYSIS

Thermal analysis is defined as a procedure of determining the temperature development in members based on the thermal actions and the material properties of the members and the protective surfaces [29].

Wood and steel have their properties changed with the temperature increase. Therefore, it is crucial to do a detailed thermal analysis of these materials in order to predict their behavior as structural members.

6.1 Modes of Heat Transfer

Heat transfer can be defined as the movement of thermal energy between two or more substances at different temperatures. Due to the temperature difference, heat transfer can occur in three different modes: conduction, convection, and radiation [29, 30].

6.1.1 Conduction

Conduction takes place when heat is transferred between solid bodies or/and stationary fluids. This mode of heat transfer occurs at the atomic level, where energy is transferred from the greater energy particles to the lower energy particles, via direct molecular collision. Heat is always transmitted from higher temperature particles to lower temperature ones [29, 30].

All heat transfer processes can be quantified in terms of appropriate rate equations. In this heat transfer mode, the equation rate is based on Fourier's law of thermal conduction. This law was formulated by Joseph Fourier, who concluded that "the heat flux resulting from thermal conduction is proportional to the magnitude of the temperature gradient and opposite to it in sign". The differential form of Fourier's law of thermal conduction is expressed in equation 26,

$$q'' = -\lambda \nabla \mathrm{T} \tag{26}$$

where the vector q'' is the heat flux $\left[\frac{W}{m^2}\right]$, λ is the thermal conductivity of the material $\left[\frac{W}{m.K}\right]$, and $\nabla \mathrm{T}$ is the temperature gradient $\left[\frac{K}{m}\right]$ [29, 30].

For a unidirectional conduction process, this observation may be expressed as:

$$q'' = -\lambda \frac{\partial \mathrm{T}}{\partial \mathrm{x}} \tag{27}$$

where $\frac{\partial \mathrm{T}}{\partial \mathrm{x}}$ is the temperature gradient $\left[\frac{K}{m}\right]$ in the direction of heat flow. [29, 30].

6.1.2 Convection

Convection can be defined as the transmission of heat through a fluid (liquid or gas), that is in motion, caused by the actual movement of the warmed substance. The faster the fluid motion, the greater the amount of heat transferred via convection [29, 30].

Convective heat transfer can be classified according to the nature of the fluid flow. If the fluid is forced into motion by any external system to the fluid, i.e. fans or pumps, over the solid surface, it is referred to as forced convection. On the other hand, if the fluid is forced into motion by buoyancy forces, induced as a result of changes in density due to the temperature changes of the fluid, it is referred to as free convection or natural convection [29, 30].

The rate of heat transfer for convection is given by Newton's Law of cooling.

$$q'' = h_c(T_s - T_\infty) \tag{28}$$

where the vector q'' is the heat flux $\left[\frac{W}{m^2}\right]$, h_c is the convection heat transfer coefficient $\left[\frac{W}{m^2.K}\right]$, T_s is the surface temperature $[\mathrm{K}]$, and T_∞ is the fluid temperature $[\mathrm{K}]$.

6.1.3 Radiation

Thermal radiation is electromagnetic radiation emitted by all material above a temperature of absolute zero due to the thermal motion of atomic particles. This method of heat transfer does not require a medium for the process to occur, and no mass is exchanged [29, 30].

The heat flux that is transmitted in the presence of radiation is obtained by the law of Stefan Boltzmann (fundamental law of radiation), according to equation 29.

$$q' = \varepsilon \times \sigma \times \mathrm{A} \times T_s^4 \tag{29}$$

where the vector q' is the heat transferred per unit time $[\mathrm{W}]$, ε is the emissivity of the surface (dimensional 0-1), the typical emissivity values of steel and wood are, respectively, $\varepsilon = 0{,}7$ and $\varepsilon = 0{,}8$, σ is the Stefan-Boltzmann constant, $5{,}6697 \times 10^{-8}\left[\frac{W}{m^2.K^4}\right]$, A is the heat transfer area $[m^2]$, and T_s is the absolute surface temperature $[^{\mathrm{O}}C]$ [29, 30].

6.2 Fire curve

One of the most critical factors for the study of exposed elements in fire situations is the characterization of the fire itself. For a fire situation, a standard curve refers to the time-temperature used in tests for defining the fire rating of elements in general. The International Standards Organization's standard (ISO834) defines the time-temperature curve by equation 30,

$$\mathrm{T} = \mathrm{T}_0 + 345\log_{10}(8t + 1) \tag{30}$$

Where T is the fire temperature evolution $[^{\mathrm{O}}C]$, T_0 is the initial temperature, usually $20^{\mathrm{O}}C$, and t is the time $[min]$ [31].

6.3 Numerical Thermal Analysis

6.3.1 Equations and boundary conditions for heat transfer

Thermal analysis allows to know the temperature distribution and to understand the heat transfer processes that occur in a body. The heat conduction is given by a second order differential equation that admits some boundary conditions in its solution. Equation 31 governs the conduction of heat in solids [32, 33].

$$\frac{\partial}{\partial x}\left(\lambda\frac{\partial T}{\partial x}\right) + \frac{\partial}{\partial y}\left(\lambda\frac{\partial T}{\partial y}\right) + \frac{\partial}{\partial z}\left(\lambda\frac{\partial T}{\partial z}\right) + \dot{\mathrm{Q}} = \rho C_p\frac{\partial T}{\partial t} \tag{31}$$

Where λ is the thermal conductivity $\left[\frac{W}{m.K}\right]$, ρ is the material density $\left[\frac{kg}{m^3}\right]$, C_p is the heat capacity $\left[\frac{kJ}{kgK}\right]$. $\dot{\mathrm{Q}}$ is the internal heat-generation rate per unit volume and time $\left[\frac{J}{m^3 s}\right]$.

In order to solve equation 31, it is necessary to define the initial conditions and the boundary condition appropriately for the problem in the study, as represented in equations 32 to 35. A temperature field that satisfies the differential equation for heat conduction shall together satisfy the initial condition and the boundary conditions. The initial condition refers to the temperature at the initial instant (t = 0) and the boundary conditions relate to temperatures or heat flows on certain surfaces of the solid. The boundary conditions of the problem consist of an exchange of energy with the surroundings, and the energy flow at the boundary comprises radiation and convection [29, 32, 33].

- **Dirichlet boundary condition,** a condition in which temperatures are prescribed in a part of the boundary [32, 33].

$$T = \overline{T} \quad in \ \Gamma_T \tag{32}$$

- **Neumann boundary condition,** a condition corresponding to an initially specified flow in the part of the boundary Γ_q, being n the normal vector outside that boundary [32, 33].

$$q = -\lambda \frac{\partial T}{\partial n} = \bar{q} \quad in \ \Gamma_q \tag{33}$$

- **Cauchy boundary condition,** convective heat flow q_e, between a part Γ_c of the boundary at temperature T, and the environment at temperature T_∞ [32, 33].

$$q_e = -\lambda \frac{\partial T}{\partial n} = h_c \ (T - T_\infty) \ \ in \ \Gamma_c \tag{34}$$

- Radioactive heat flow q_r, between a part Γ_r of the boundary at temperature T, and the surroundings at temperature T_s [32, 33].

$$q_e = -\lambda \frac{\partial T}{\partial n} = h_r \ (T - T_s) \ \ in \ \Gamma_r \tag{35}$$

The initial temperature in the numerical model was considered to be uniform and equal to 20 ºC. The external surface of the connection is exposed to the standard fire curve ISO834 for 60 minutes. Also, the convection and radiation boundaries were defined for the external surface, where the convection coefficient is 25 [W/m^{2}K], and the emissivity of the fire is constant and equal to 1 [21].

6.3.2 Finite Element Method

Using the finite element method to discretize the problem in the domain, in order to choose the weighting functions, a weak formulation based on the *Galerkin* method

was used. This enables to obtain the following system of differential equations represented in equation 36 or 37 [32, 33].

$$\mathbf{K}_{(\lambda)(T,t)}\mathbf{T}_{(t)} + \mathbf{C}_{(C_p,\rho)}\dot{\mathbf{T}}_{(t)} = \mathbf{F}_{(T,t)(Q,q,h_c,T_p)} \tag{36}$$

$$\mathbf{KT} + \mathbf{C}\dot{\mathbf{T}} = \mathbf{F} \tag{37}$$

Each term of equation 37 might be represented in terms of the following expressions.

$$\mathbf{K}_{ij} = \sum_{e=1}^{E}\int_{\Omega^e}\left(\nabla\mathbf{N}_i\boldsymbol{\lambda}\nabla\mathbf{N}_j\right)d\Omega^e + \sum_{e=1}^{n}\int_{\Gamma_h^e}\left(h_{cr}\mathbf{N}_i\mathbf{N}_j\right)d\Gamma_h^e \tag{38}$$

$$\mathbf{C}_{ij} = \sum_{e=1}^{E}\int_{\Omega^e}\left(\rho C_p\mathbf{N}_i\mathbf{N}_j\right)d\Omega^e \tag{39}$$

$$\mathbf{F}_{ij} = \sum_{e=1}^{E}\int_{\Omega^e}\left(\mathbf{N}_i\dot{\mathrm{Q}}\right)d\Omega^e - \sum_{e=1}^{p}\int_{\Gamma_h^e}\left(\mathbf{N}_i\bar{\mathrm{q}}\right)d\Gamma_q^e + \sum_{e=1}^{n}\int_{\Gamma_h^e}\left(h_{cr}\mathbf{T}_\infty\mathbf{N}_i\right)d\Gamma_h^e \tag{40}$$

Where E is the total number of elements, n is the number of elements with boundary type Γ_h , p is the number of elements with boundary type Γ_q, $d\Gamma_q^e$ and $d\Gamma_h^e$ represent the line elements, and $\mathbf{N}_i$ and $\mathbf{N}_j$ are typical shape functions [32, 33].

Using a finite difference technique to discretize the time, the system of ordinary differential equations 37 results in equation 41 [32, 33].

$$\widehat{\mathbf{K}}_{n+\alpha}\mathbf{T}_{n+\alpha} = \widehat{\mathbf{F}}_{n+\alpha} \quad 0 < \alpha \leq 1 \tag{41}$$

Where,

$$\widehat{\mathbf{K}}_{n+\alpha} = \mathbf{K}_{n+\alpha} + \frac{1}{\alpha\Delta t}\mathbf{C}_{n+\alpha} \tag{42}$$

$$\widehat{\mathbf{F}}_{n+\alpha} = \mathbf{F}_{n+\alpha} + \frac{1}{\alpha\Delta t}\mathbf{C}_{n+\alpha_n} \tag{43}$$

Having solved the system of equations 41 for $\mathbf{T}_{n+\alpha}$, at time $t_{n+\alpha}$, the value of $\mathbf{T}$ at the end of the time interval Δt, that is, at time t_{n+1}, is given by equation 44 [32, 33].

$$\mathbf{T}_{n+1} = \frac{1}{\alpha}\mathbf{T}_{n+\alpha} + \left(1 - \frac{1}{\alpha}\right)\mathbf{T}_n \tag{44}$$

The value of the parameter α could vary using the *Crank-Nicolson* scheme with $\alpha = 1/2$, using the *Galerkin* scheme with $\alpha = 2/3$, and using the *Euler Backward* scheme for $\alpha = 1$ [32, 33].

In non-linear problems, the thermal properties of the material are temperature dependent, and the system of equations represented in equation 37 may be described as shown in equation 45 [32, 33].

$$\mathbf{K}_{(T,t)}\mathbf{T}_{(t)} + \mathbf{C}_{(T,t)}\dot{\mathbf{T}}_{(t)} = \mathbf{F}_{(T,t)} \tag{45}$$

In order to completely satisfy these non-linear conditions of the problem, it is necessary to utilize an iterative procedure in each time step. In this work, a modified *Newton-Raphson* method was adopted in order to solve the thermal and transient problem with the considered time interval for each step equal to 10 s. During any step, i, of the iterative process of solution, the equation may be satisfied only if convergence is obtained. Therefore, a system of residual forces $\boldsymbol{\psi}$ will occur, shown in equation 46 [32, 33].

$$\boldsymbol{\psi}_{n+a}^{i} = \widehat{\mathbf{F}}_{n+a}^{i} - \widehat{\mathbf{K}}_{n+a}^{i}\widehat{\mathbf{T}}_{n+a}^{i+1} \neq 0 \tag{46}$$

The adjusted solution may be calculated through equation 47.

$$\Delta\mathbf{T}_{n+a}^{i} = [\widehat{\mathbf{K}}_{n+a}]^{-1}\boldsymbol{\psi}_{n+a}^{i} \tag{47}$$

The improved value of $\Delta\mathbf{T}_{n+a}^{i}$ may be achieved. Until the solution converges to the non-linear solution, the iterative procedure is continued, solving a set of linearized equations at each iteration step. The convergence criteria used is as shown in equation 48 [32, 33].

$$\frac{\left\|\Delta\mathbf{T}_{n+a}^{i}\right\|}{\left\|\Delta\mathbf{T}_{n+a}^{i+1}\right\|} < TOL \tag{48}$$

Where TOL is the specified tolerance, $\|\quad\|$ denotes the Euclidean vector norm, $\Delta\mathbf{T}_{n+a}^{i}$ is the temperature change on the i^{th} iteration, and $\Delta\mathbf{T}_{n+a}^{i+1}$ is the current temperature value [32, 33].

6.3.3 Geometry

Due to the geometry symmetry, the numerical calculation was performed using the two-dimensional cross-sections, representing a section in wood or in wood-steel material for unprotected and protected connections, figure 18 [34].

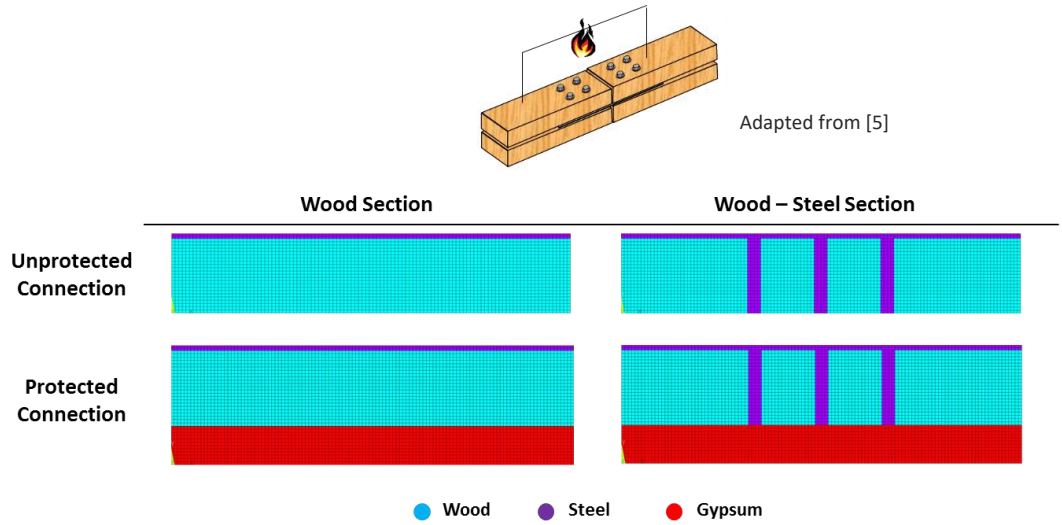

Figure 18 - Cross-sections used in the numerical calculation

6.3.4 Material Properties

The main thermal properties of a material are its thermal conductivity, density, and specific heat. The nonlinearity due to the thermal properties dependence was introduced in the numerical simulation. The material properties necessary to input in the numerical model for the W-S-W connections were described in Chapter 3.

6.3.5 Mesh and Element Type

A thermal element type is chosen for heat transfer analysis, represented in figure 19. In the ANSYS Academic Mechanical® material library, this element is denoted by *PLANE77,* and it is a two-dimensional thermal plane element with eight nodes and one single degree of freedom, temperature, at each node [35].

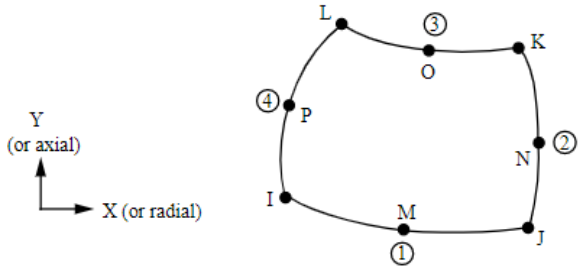

Figure 19 – Finite element *PLANE77* geometry [35]

Each node shown in figure 20 has a shape function N_i. These functions are defined by the position of the node relative to the selected element. The variation of the natural coordinates ξ, η (-1 ≤ ξ ≤ 1 -1 ≤ η ≤ 1) changes the function N_i of the respective node. The represented nodes are considered isoparametric, i.e., the geometry and the temperature field are specified in a parametric form and are interpolated with the same functions [32, 33].

For nodes, I, J, K and L, the function is given by equation 49.

$$N_i = \frac{1}{4}(1+\xi_0)(1+\eta_0) - \frac{1}{4}(1-\xi^2)(1+\eta_0) - \frac{1}{4}(1+\xi_0)(1-\eta^2) \quad (49)$$

For nodes M and O, equation 50 and 51 is used.

$$N_M = \frac{1}{2}(1-\xi^2)(1-\eta_0) \quad (50)$$

$$N_O = \frac{1}{2}(1-\xi^2)(1+\eta_0) \quad (51)$$

For nodes P and N, equation 52 and 53 is applied.

$$N_P = \frac{1}{2}(1-\xi_0)(1-\eta^2) \quad (52)$$

$$N_N = \frac{1}{2}(1+\xi_0)(1-\eta^2) \quad (53)$$

In the above equations, ξ_i and η_i are local coordinate values, and ξ, η are coordinate values in the nodes [32, 33, 35].

The mesh convergence tests were carried out to minimize the computational error. A regular mesh was considered with a size finite element equal to 2 [mm]. Both protected and unprotected connections have the same regular mesh [34].

RESULTS AND DISCUSSION

7 RESULTS AND DISCUSSION

All the represented results in the current chapter were obtained for one connection type, using the wood type GL24H and the dowel's diameter of 8 mm. All the results obtained to the remained connections are represented in the annexes.

7.1 Mechanical Design

With all design equations for room temperature, a worksheet was developed to allow the calculation of different W-S-W connections. Different parameters were considered, such as three dowel diameters, three applied tensile loads, and three wood materials.

In figure 20 the relationship between the applied load and the number of dowels required in the W-S-W connection is represented. The obtained results enable to verify a linear correlation between these parameters, with a higher increase for lower dowels diameter. As expected, the number of fasteners increases with load, as stated in the standards at room temperature. Lower dowels diameter has a higher pronounced effect in the needed of the number of fasteners. The effect due to the strength of material for GL20h, GL24h, and GL32h is less predominant. However, it is still noticeable the increase of the needed number of fasteners for lower density woods.

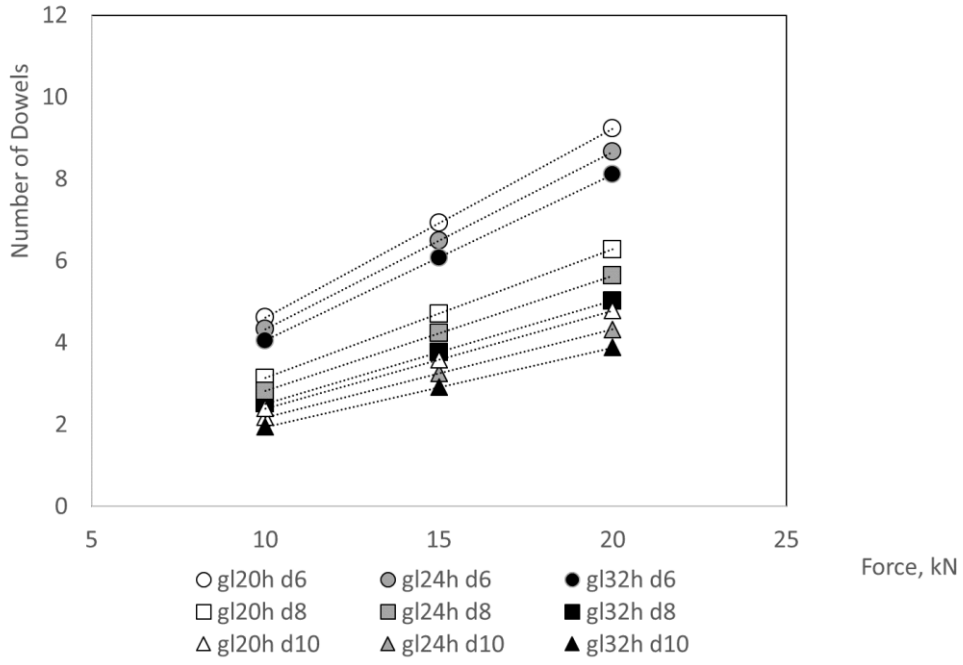

Figure 20 - Relationship between the applied load (kN) and the number of dowels

The connections obtained by the design method described in Eurocode 5, 1-1 [28], can be founded in the tables in Annex 1. In the tables mentioned, it is possible to verify the overall connections dimensions according to the different variables. Table 10 is a example from Annex 1.

Table 10 - Connection's dimensions for the mechanical design

Load (kN)	Dowel (mm)		Dowel arrangement		Distances (mm)				Connection dimensions (mm)				Tensile Stress (N/mm^2)	Characteristic load-carrying (N)
	d	length	Lines	Columns	a1	a2	a3,t	a4,c	t1	ts	H	L	$F_{t,o,d}$	$F_{v,Rd}$
10	8	186	2	3	40	24	24	80	45	6	7	400	12,288	3548,4
15	8	186	2	3	40	24	24	80	45	6	7	400	12,288	3548,4
20	8	186	2	3	40	24	24	80	45	6	7	480	12,288	3548,4

7.2 Thermal Analysis

According to Eurocode 5 part 1-2 [21], the wood carbonizes when it reaches a temperature of 300^{o}C. Above that, the wood does not present any mechanical resistance, which gradually reduces the load capacity of the structural elements according to the char layer depth progress.

7.2.1 Unprotected connections

The relationship between the char layer thickness and its respective fire time instant provides the wood charring rate. This quantity is essential in the analysis of the wood char layer since it presents the rate or quantity of wood (in millimeters) that is being charred per unit of time (minutes).

In this research, the determination of the charring rate was performed in order to obtain numerical validation for the considered models in comparison with the Eurocode 5, part 1-2 [21]. According to this, the charring rate is calculated in three different locations of the numerical model, considered as the most relevant controlled points. In figure 21, the numerical model is represented with his mesh and the control points which are: faraway of the dowels (point k1), in the vicinity of the dowel (point k2), and between two dowels (point k3).

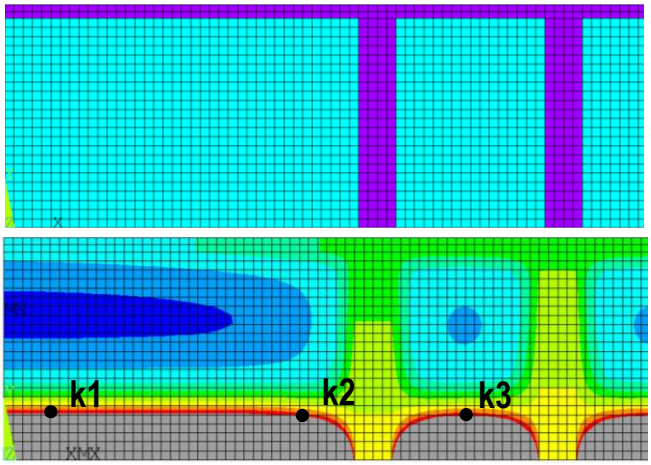

Figure 21 - Representation of the studied points in the mesh model

In table 11, different values of the charring rate are shown for the respective points as well as for the three types different of the wood. All the remain connections values are exposed in Annex 2.

Table 11 - Charring rate for the points in consideration based on the type of wood [mm/min]

Point	GL20H	GL24H	GL32H
k1	0,80	0,75	0,7
k2	0,77	0,7	0,66
k3	0,79	0,71	0,69

The results show that the connections present a char layer with nonlinear variation after the fire exposure. Using only the Eurocode 5 part-1-2 [21], it is impossible to understand the fire effect through and inside the connection. The charring rate is considered as a standard and constant value, however using the numerical results, the charring rate varies in the connection, due to the effect of the steel and the wood density.

Eurocode 5 suggests a charring rate equal to 0.65 mm/min or 0.7 mm/min for softwood or hardwood, with density higher than 290 kg/m^3. With that said, since it is used a hardwood in the connection its safe to say that higher wood densities have a closer value of charring rate. In conclusion and according to the results, when wood density increases the charring rate decrease. The point k3 has a higher difference of values due to the different distances between the dowels imposed by the mechanical design.

Figure 22 represents the temperature evolution over fire exposure during 60 minutes, measured in the external points (k1e, k2e, k3e, k4e) and the internal points (k1i, k2i, k3i, k4i) of an unprotected connection. All the remain connections values are exposed in Annex 3.

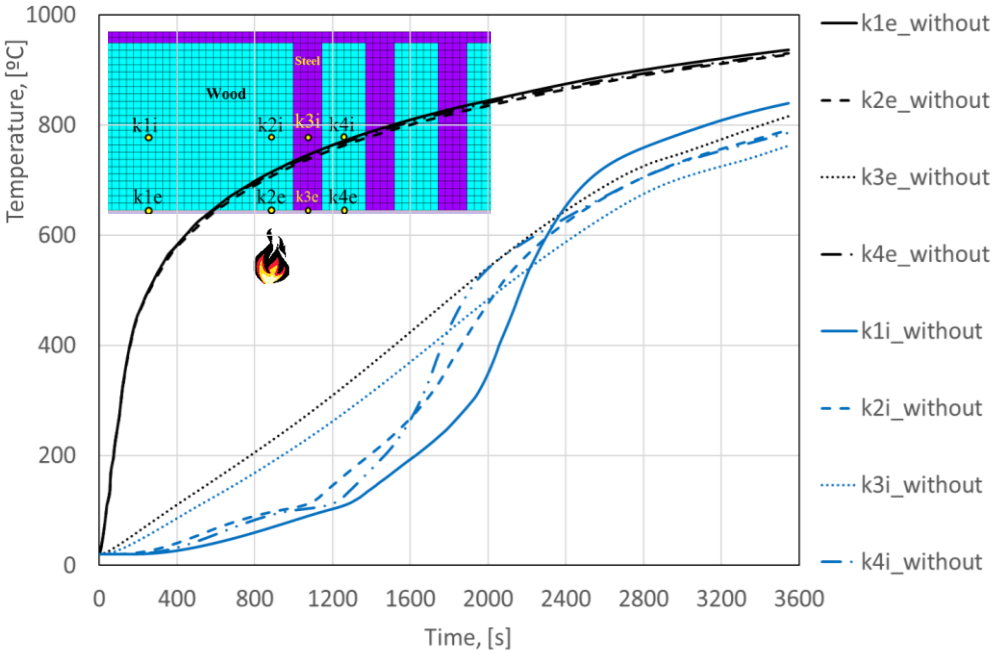

Figure 22 – Time-temperature history during 60 minutes, measured for the external and internal points of an unprotected connection

Through the analysis of figure 22, it is possible to observe that the external keypoints (k1e, k2e, k4e) have the same behavior as the ISO834, which is expected to happen because there is no protection. On the other hand, the external point k3e has a different behavior from the other external points, which happens due to the steel thermal conductivity effect.

The internal keypoint k3i has the same behavior as the external keypoint k3e since they are both in the steel dowel, the only difference is in the temperature field being higher for the external point since it is closer to the fire.

Overall, it is noticeable a considerable difference between the internal and the external keypoints. This phenomenon occurs due to the wood char layer effect that allows keeping the connection core at a lower temperature.

For the internal keypoints, the ones in the vicinity of the steel dowels (k2i, k4i) have higher temperatures as expected because the steel dowels bring heat inside the connection.

Figure 23 presents the numerical results of the temperature development at two different fire time instants (20 and 30min) in the unprotected connection, comparing the three wood densities. The blue zone represents the wood material, violet represents the steel material, and grey color represents the char layer on the wood. This phenomenon is considered in the numerical model according to the criterion of char layer formation applied by the isothermal of 300 ^{o}C. All the remain connections values are exposed in Annex 4.

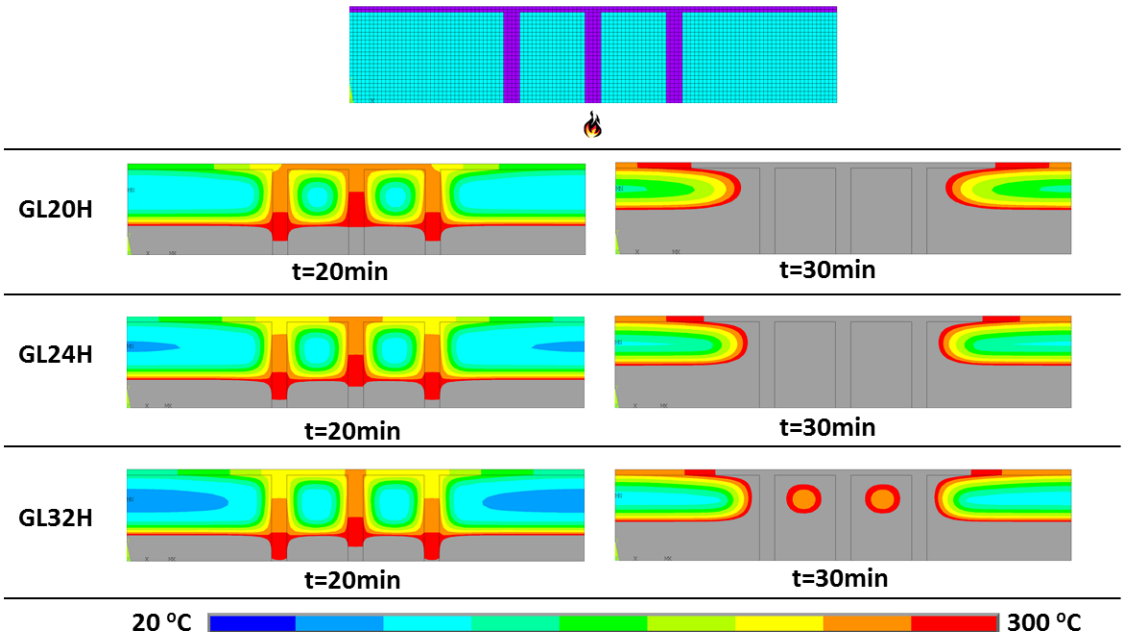

Figure 23 - Temperature development at two different fir time instants (15 and 30 min) in the unprotected connection included all three wood densities

According to Eurocode 5, part 1-2 [21], the steel dowel time of fire resistance ($t_{d,fi}$) is 20 minutes. This is confirmed by the figure because the steel dowels are already at temperature close to 300^{o}C in this instance, undermining the whole connection resistance. This happens due to the thermal conductivity of the steel, which increases the temperature field of the wood in the vicinity of the fasteners.

At the 30 minutes mark, the connection is not operational despite what is said in Eurocode 5, part 1-2 [21]. According to the figure it is visible that the wood between fasteners fully achieves temperatures higher than the carbonization temperature of the wood (300^{o}C). This inconsistency of the obtained results shows the importance of these numerical simulations, that represent the impact of the use of the steel elements.

The heat conduction and the char layer evolution inside the wood with lower density occurred with more pronounced. The steel plate as the internal member remains at a lower temperature if the exposure time is small, but increases when fire exposure increases, and near the steel dowels. At elevated temperatures the steel dowels

promote heat up quickly inside the wood connection, they lose their stiffness after 100°C and strength after 400°C and cause a wood charring layer faster.

7.2.2 Protected Connections

In this section, the protected connections are analyzed with gypsum plates as the insulation material. For the protected connections gypsum type A and type F will be used, with a thickness of 23mm and 18mm respectively, according to the procedure identified in section 5.1.2. With the obtained numerical results, it was possible to observe different thermal behaviors based on the use of different gypsum types.

Figure 24 presents the numerical results of the temperature development at 60 minutes in the protected connection, comparing the two used gypsum types. The grey color represents the thickness *hp* of the gypsum panel (A or F) with a temperature above 300°C. All the remain connections values are exposed in Annex 5.

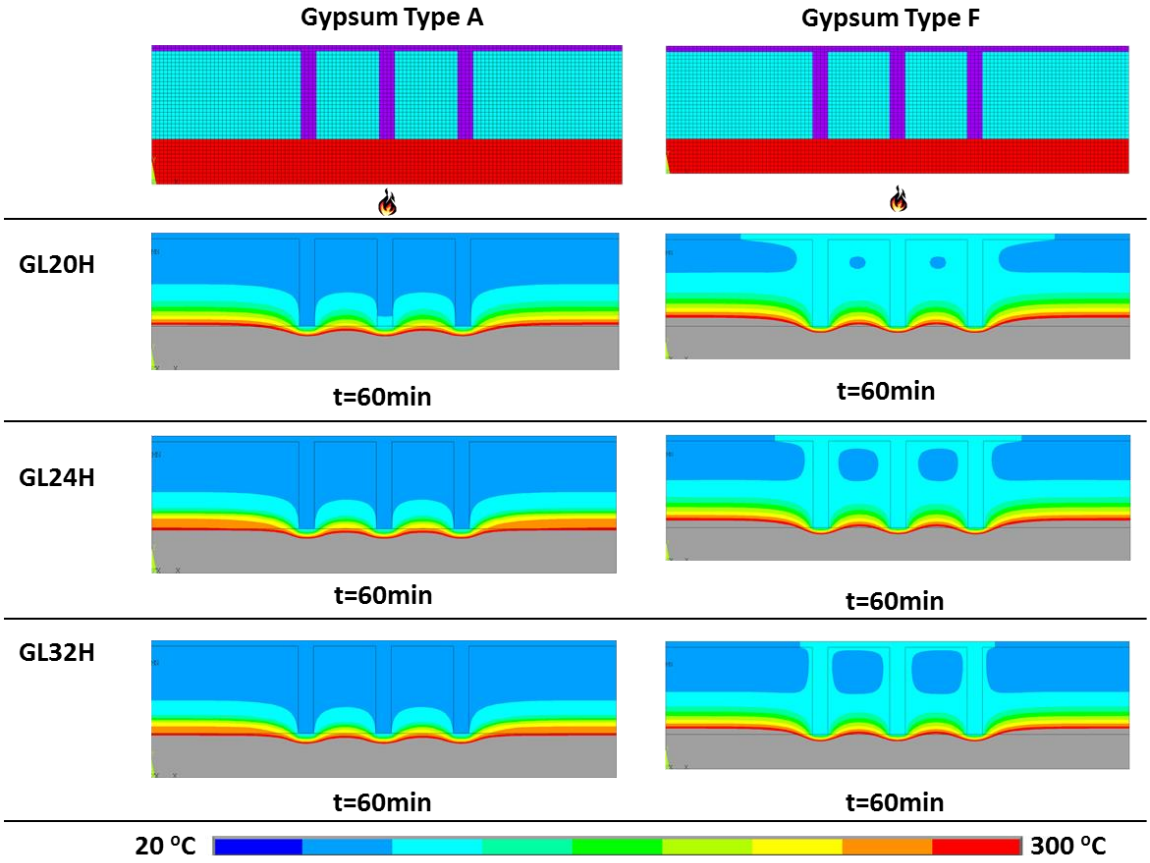

Figure 24 - Temperature development at 60 minutes in the protected connection using Gypsum Type A and F

Gypsum type F has a lower thickness than type A, and in general protect the wood, but produces higher temperatures, increasing with the lower wood density. In general, both gypsum panels are a great thermal protection of the wood connections for a required standard fire resistance period of 60 min. The numerical results demonstrate

that the used material properties for the gypsum plasterboards have a great performance with the minimum imposed by the design thickness of each panel according to the standards.

Figure 25 represents the temperature evolution over time of 60 minutes for the measured external points (k1e, k2e, k3e, k4e) and the internal points (k1i, k2i, k3i, k4i). With the obtained results it is clear that the following connection is well designed for a fire exposure of 60 minutes. The external points (k2e, k4e) have lower temperatures than 300ºC, which means that the charring rate of the wood did not start. The higher temperature of the connection is around 300ºC for the external point (k1e) at the end of the numerical simulation, which just started the charring layer. All the remain connections values are exposed in Annex 3.

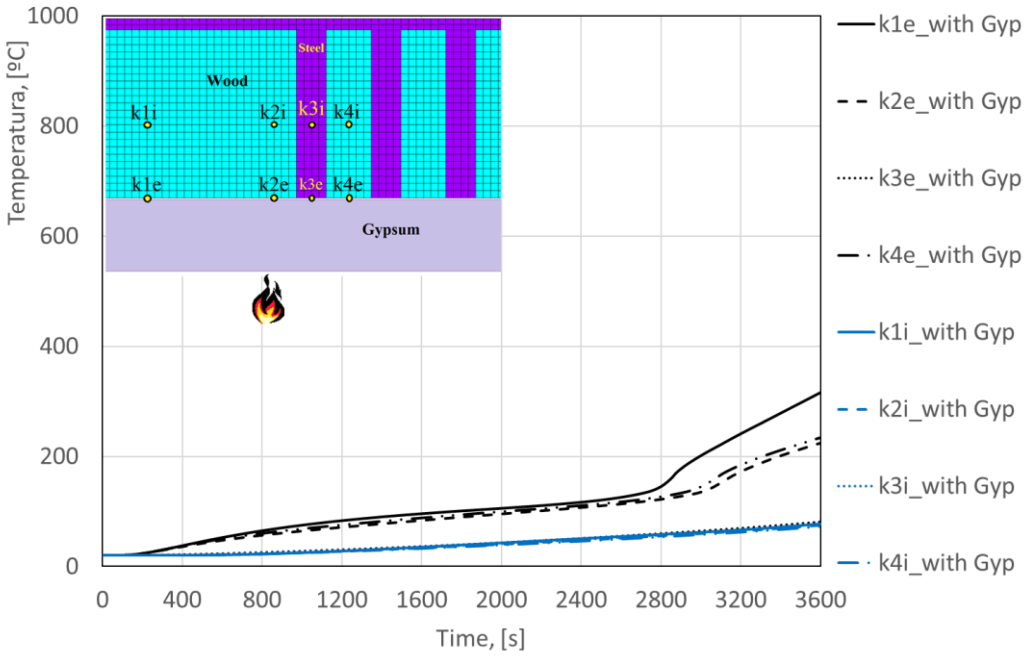

Figure 25 - Temperature progression over time of 60 minutes for the external and internal points

In figure 26 and 27, it is represented a comparison between the different protected connections, one using gypsum type A and the other using gypsum type F. Gypsum type A is used for typical applications while type F is used on fire situations. Therefore, employing this analysis, it is possible to assess the impact of using two different gypsum types as an insulator. All the remain connections values are exposed in Annex 6.

For the external points (k1e, k2e, k3e, k4e), figure 26, we can conclude that using a smaller thickness of the gypsum type F plasterboard causes a lower resistance to the fire. Around the 2400s there is the turning point where the gypsum loses his resistance

while the gypsum type A it is around 2800s. Also, the temperature range is higher for the less resistance material, which is the type F, and both types have similar temperature evolution over time.

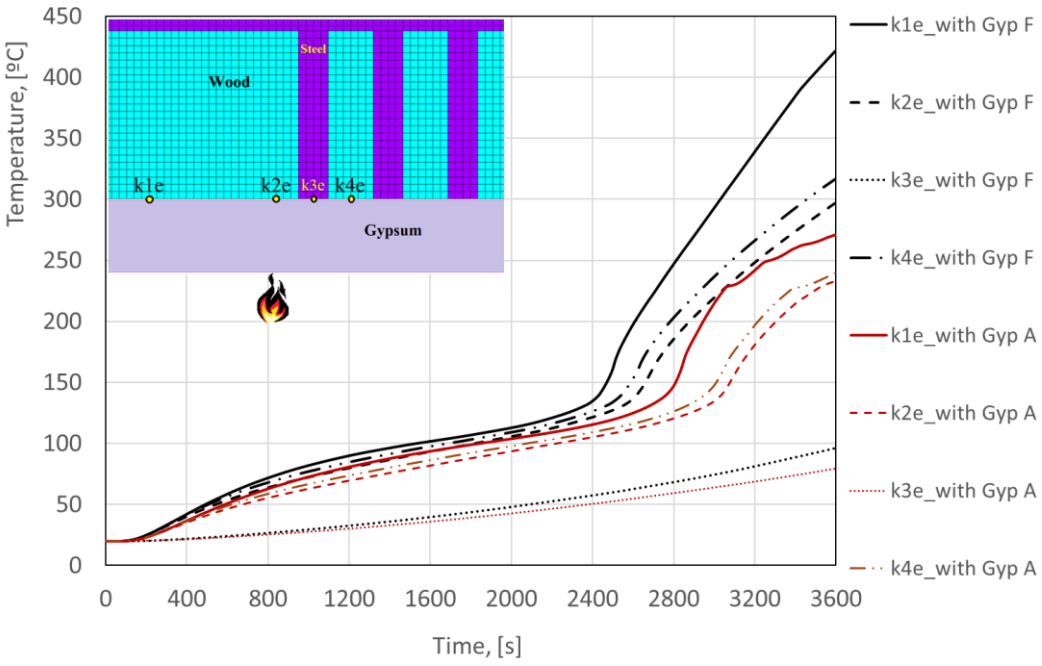

Figure 26 – Comparison between Gypsum Type A and F for the external points

For The internal points (k1i, k2i, k3i, k4i), figure 27, they have the same temperature development when exposed to fire, the difference is that the gypsum type F has higher temperatures which are expected since the thickness of the plasterboard is smaller.

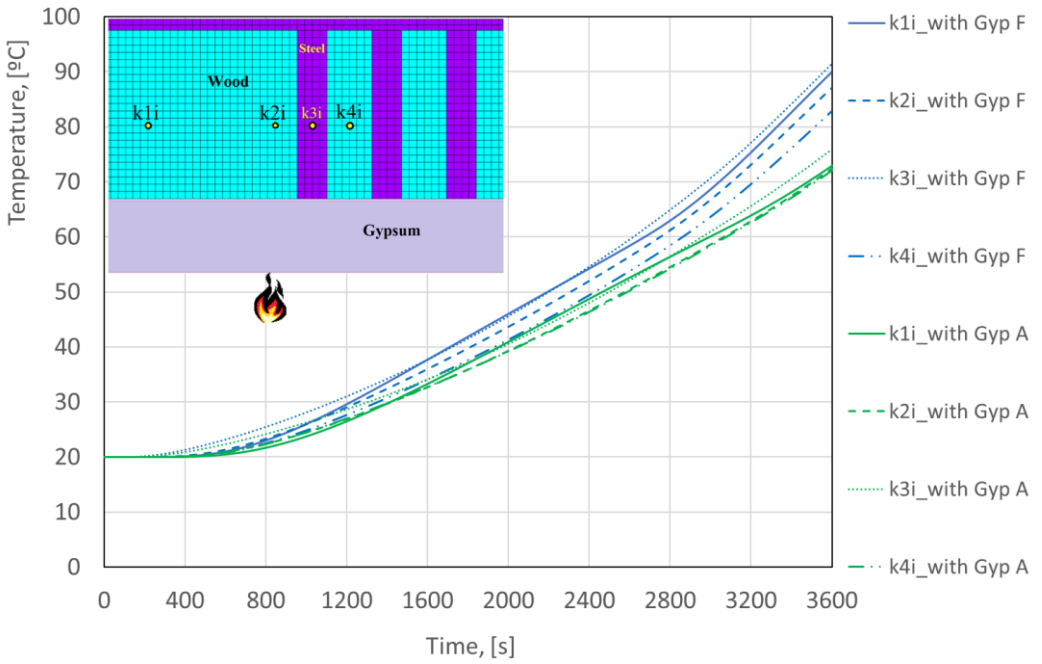

Figure 27 - Comparison between Gypsum Type A and F for the internal points

Figures 28 and 29 show the temperature evolution between the unprotected and the protected connections with gypsum type A for the external and internal points. While the unprotected connections have the same behavior as the ISO834, the protected ones are designed to maintain the connection stable for 60 minutes. All the remain connections values are exposed in Annex 7.

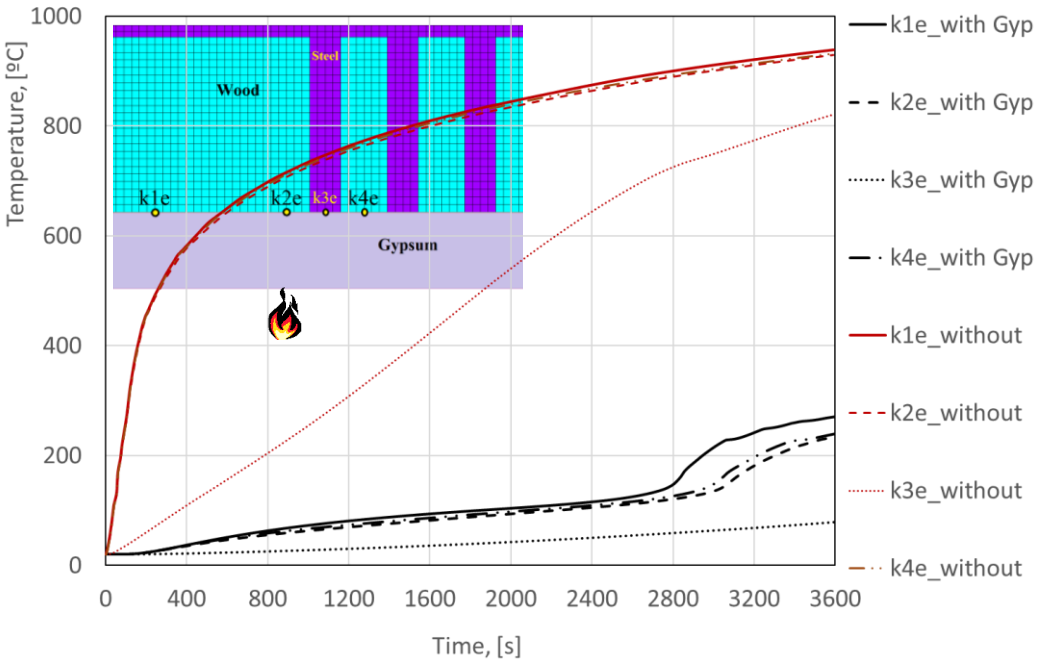

Figure 28 - Comparison between the unprotected and protected connections for the external points

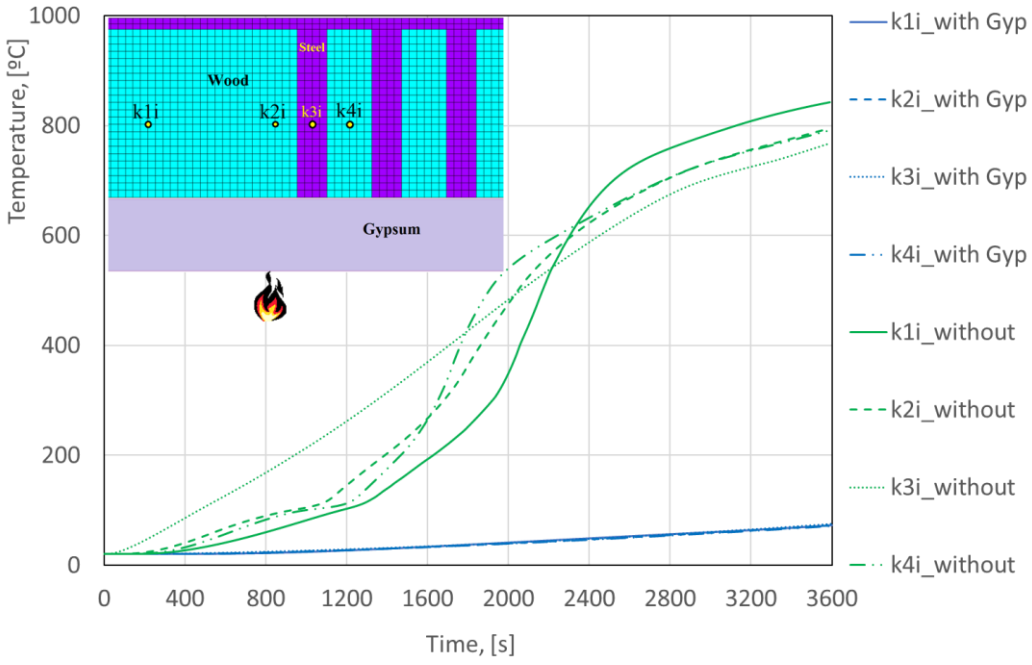

Figure 29 - Comparison between the unprotected and protected connections for the internal points

CONCLUSIONS AND FUTURE WORK

8 CONCLUSIONS AND FUTURE WORK

8.1 CONCLUSIONS

All purposes tasks of the present master thesis were achieved. Therefore, the most relevant conclusions are the following:

- The number of fasteners increases with the applied load according to standards at room temperature. Lower dowels diameters enhance the effect of the number of fasteners used in the connection with the increasing of the applied tensile load.

- According to the standards, the charring rate is considered as a constant value in all the wood connection. However, based on numerical results, it is verified that the charring rate varies due to steel heat conduction and the wood density effect. The calculated charring rate for cross-sections only in wood approximates the values proposed by the Eurocode. Nevertheless, there is a variation of values for different wood densities.

- The inclusion of steel, such as dowel material or an internal plate, induces internal heating after fire exposure. For this reason, the charring rate of wood increases in the vicinity of the steel. The internal plate produces also an increasing effect of this heat. It is essential to point out that steel provides heat flow to the inside of the connection, but the wood elements in the vicinity provide some insulation when the fire is starting. It was possible to observe that, both materials participate in the evolution of the char layer in the W-S-W connection.

- The passive fire protection with gypsum plasterboards is an option that guarantees the connection safety. The obtained results with the numerical model show the connection ability to fire resistance with the calculated panel thickness. It is also possible to verify that the properties adopted for the two types of gypsum chosen from the literature were calibrated since they guarantee the time of fire resistance of the designed W-S-W connection.

- Using only the Eurocode 5 part 1-2 [21], it is not possible to predict the fire evolution through and inside the connection.

- The numerical model gives an acceptable prediction of the fire resistance in W-S-W connections. The main objective was to obtain an alternative methodology, which allows the measuring of the fire resistance in different types and sizes of connections during a standard fire.

8.2 FUTURE WORK

This thesis allowed to observe some relevant conclusions regarding the behavior of wood connections under fire conditions. However, this subject provides an infinity of different situations that can be analyzed.

In order to generate new knowledge and continue the scientific research, some interesting situations are highlighted for future work:

- Increase the gap between the parameters under consideration, i.e. higher density values differences in the wood types, higher difference between the dowel diameters used.

- The use of mechanical loads simultaneously with the fire action, for thermomechanical investigation;

- Perform different experimental tests for both mechanical and thermal behavior to correlate the results with the numerical analysis.

REFERENCES

9 REFERENCES

1. Kuklík, P., *History of Timber Structures*, in *Handbook 1 - Timber Structures* E.M.f.D.a.T.o.T. Structures, Editor. 2008, Leonardo da Vinci Pilot Projects: Czech Technical University in Prague.
2. Laboratory, F.P., *Wood Handbook - wood as an engineering material* Centennial Edition ed. 2010, Madison, Wisconsin - U.S.: USDA - U.S. Department of Agriculture.
3. João Negrão, A.F., *Projecto de Estruturas de Madeira*, ed. E.T. Publindústria. 2009, Portugal.
4. M. Tavakkol-khah, W.K., *Calculation Model for Predicting Fire Resistance Time of Timber Members* Fire Safety Science, 1997. **5**: p. 1201-1211.
5. Lei Peng, G.H., Jim Mehaffey, Mohammad Mohammad, *Predicting the Fire Resistance of Wood–Steel–Wood Timber Connections.* Fire Technology, 2011. **47**(4): p. 1101-1119.
6. Peng, L., *Performance of heavy timber connections in fire*, in *Department of Civil and Environmental Engineering*. 2010, Carleton University: Canada.
7. Elza M. M. Fonseca, P.A.S.L., Lino Silva, *Fire Safety of Wood-Steel Connections*, in *SYMCOMP 2019*. 2019: Porto, Portugal.
8. Michael Dorn, K.d.B., Josef Eberhardsteiner, *Experiments on dowel-type timber connections.* Engineering Structures, Elsevier, 2013. **47**: p. 67-80.
9. Palma, P., *Fire behaviour of timber connections*, in *Dept. of Civil, Environmental and Geomatic Engineering (D-BAUG)*. 2016, Institute of Structural Engineering (IBK) Zurich
10. C. Maraveas, K.M., Ch. E. Matthaiou, *Performance of Timber Connections Exposed to Fire: A Review.* Fire Technology, 2013. **51**(6): p. 1401-1432.
11. Andrea Frangi, C.E., Mario Fontana, *Experimental fire analysis of steel-to-timber connections using dowels and nails.* FAM: Fire and Materials, 2009. **34**(1): p. 1-19.
12. G. Hochreiner, T.K.B., M. Schweigler, J. Eberhardsteiner, *An Engineering Modeling Approach for the Nonlinear Load-Displacement Behaviour of Single Dowel Connections – Parameter Study*, in *World Conference on Timber Engineering (WCTE 2016)*. 2016: Vienna, Austria.
13. Maxime Audebert, M.T., Abdelhamid Bouchair, Dhionis Dhima, *Thermal and thermo-mechanical behaviour of timber connections in fire.* Cost action C26:Urban Habitat Constructions under Catastrophic Events - Proceeding of the Final Conference, 2010: p. 189-194.

14. Simon Schnabl, G.T., *Coupled heat and moisture transfer in timber beams exposed to fire*, in *9th World Conference on Timber Engineering 2006*. 2006.
15. Karim Ghazi Wakili, E.H., *Four Types of Gypsum Plaster Boards and their Thermophysical Properties Under Fire Condition.* Journal of Fire Sciences, 2009. **27**(1): p. 27-43.
16. Jorge M.Branco, T.D., *Analysis and strengthening of carpentry joints.* Constrution and Building Materials, 2015. **97**: p. 34-47.
17. Chuang Miao, D.F., Michael T. Heitzmann, Henri Bailleres, *GFRP-to-timber bonded joints: Adhesive selection.* International Journal of Adhesion and Adhesives, 2019. **94**: p. 29-39.
18. Martin Sviták, M.G., Jan Penc, *Heat Resistance of Glued Finger Joints in Spruce Wood Constructions.* Bioresources, 2014. **9**(4): p. 7529-7541.
19. Daniels, N., *Structural Drawing*. 2018.
20. Timber, H.N., *Glued Laminated Timber*, H. group, Editor. 2019: Austria.
21. Standardization, CEN, *Eurocode 5: Design of timber structures - Part 1-2: General - Structural fire design*, in *EN 1995-1-2* 2004: Brussels.
22. Standardization, CEN, *Eurocode 3: Design of steel structures - Part 1-1: General rules and rules for buildings*, in *EN 1993-1-1*. 2005: Brussels.
23. Standardization, CEN, *Eurocode 3: Design of steel structures - Part 1-2: General rules - Structural Fire*, in *EN 1993-1-2*. 2004: Brussels.
24. I. Rahmanian, Y.W., *Thermal Conductivity of Gypsum at High Temperatures – A Combined Experimental and Numerical Approach.* Acta Polytechnica, 2009. **49**(1): p. 16-20.
25. D. J. Hopkin, T.L., J. El-Rimawi, V. V. Silberschmidt, *A numerical study of gypsum plasterboard behaviour under standard and natural fire conditions.* FAM: Fire and Materials, 2012. **36**(2): p. 107-126.
26. Andrea Frangi, V.S., Mario Fontana, Erich Hugi, *Experimental and Numerical Analysis of Gypsum Plasterboards in Fire.* Fire Technology, 2010. **46**: p. 149-167.
27. Lino Silva, Elza M. M. Fonseca, Pedro A. S. Leite, *The Density Effect in (W-S-W) Wood Connections with Internal Steel Plate and Passive Protection Under Fire* in *5CILASCI - 5º Congresso Ibero-Latino-Americano em Segurança Contra Incêndios*. 2019: Porto.
28. Standardization, CEN, *Eurocode 5: Design of timber structures - Part 1-1: General - Common rules and rules for buildings* in *EN 1995-1-1 :2004+A 1*. 2008: Brussels.
29. McGraw-Hill, *Handbook of Heat Transfer*, ed. J.R.H. Warren M. Rohsenow, Young I. Cho 1998.
30. Frank P. Incropera, D.P.D., Theodore L. Bergman, Adrienne S. Lavine, *Fundamentos de Transferência de Calor e de Massa*, ed. L.-L.T.e.C.E. S.A. 2007, Rio de Janeiro, Brazil.

31. Standardization, C.E.C.f., *Eurocode 1: Actions on structures - Part 1-2: General actions - Actions on structures exposed to fire*, in *EN 1991-1-2* 2002: Brussels.
32. Vila Real, Paulo J. M. F., *Modelação por Elementos Finitos da Solidificação e Comportamento Termo-Mecânico de Peças Vazadas em Modelações Metálicas*, in *Engenharia Mecânica*. 1993, FEUP - Faculdade de Engenharia da Universidade do Porto.
33. Fonseca, E.M.M., *Modelação numérica do comportamento termo-mecânico de perfis metálicos sujeitos à acção do fogo*, in *Engenharia Mecânica*. 1998, FEUP-Faculdade de Engenharia da Universidade do Porto.
34. Elza M. M. Fonseca, L. Silva, Pedro A. S. Leite, *Numerical model to predict the effect of wood density in W-S-W connections with and without passive protection under fire.* Journal of Fire Sciences, 2019.
35. ANSYS, i., *Theory Reference - Release 5.6*, ed. P.K. Ph.D. 1999, U.S. .

ANNEXES

10 ANNEXES

10.1 ANNEX 1

In Annex 1 is shown the main dimensions for all connections obtained by the mechanical design.

Load (kN)	Dowel (mm)		Dowel arrangement		Distances (mm)				Connection dimensions (mm)				Tensile Stress (N/mm^2)	Characteristic load-carrying (N)
	d	length	Line	Column	a1	a2	a3,t	a4,c	t1	ts	H	L	$F_{t,o,d}$	$F_{v,Rd}$
GL20H														
10	6	186	2	3	30	18	18	80	45	6	54	440	10,24	2166,4
	8	186	2	3	40	24	24	80	45	6	72	480	10,24	3186,7
	10	186	2	3	50	30	30	80	45	6	90	520	10,24	4180,0
15	6	186	3	3	30	18	18	80	45	6	72	440	10,24	2166,4
	8	186	2	3	40	24	24	80	45	6	72	482	10,24	3186,7
	10	186	2	3	50	30	30	80	45	6	90	520	10,24	4180,0
20	6	186	4	3	30	18	18	80	45	6	90	400	10,24	2166,4
	8	186	3	3	40	24	24	80	45	6	96	480	10,24	3186,7
	10	186	2	3	50	30	30	80	45	6	90	520	10,24	4180,0
GL24H														
10	6	186	2	3	30	18	18	80	45	6	54	440	12,29	2308,1
	8	186	2	3	40	24	24	80	45	6	72	480	12,29	3548,41
	10	186	2	3	50	30	30	80	45	6	90	520	12,29	4624,5
15	6	186	3	3	30	18	18	80	45	6	72	440	12,29	2308,2
	8	186	2	3	40	24	24	80	45	6	72	482	12,29	3548,4
	10	186	2	3	50	30	30	80	45	6	90	520	12,29	4624,5
20	6	186	3	3	30	18	18	80	45	6	90	400	12,29	2308,2
	8	186	2	3	40	24	24	80	45	6	72	480	12,29	3548,41
	10	186	2	3	50	30	30	80	45	6	90	520	12,29	4624,5
GL32H														
10	6	186	2	3	30	18	18	80	45	6	54	440	16,38	2467,5
	8	186	1	3	40	24	24	80	45	6	48	480	16,38	3982,0
	10	186	1	3	50	30	30	80	45	6	60	520	16,38	5156,7
15	6	186	3	3	30	18	18	80	45	6	72	440	16,38	2467,5
	8	186	2	3	40	24	24	80	45	6	72	482	16,38	3982,0
	10	186	1	3	50	30	30	80	45	6	60	520	16,38	5156,7
20	6	186	3	3	30	18	18	80	45	6	54	400	16,38	2467,5
	8	186	2	3	40	24	24	80	45	6	72	480	16,38	3982,0
	10	186	2	3	50	30	30	80	45	6	90	520	16,38	5156,7

10.2 ANNEX 2

Annex 2 represents the values of the charring rate for the respective points as well as the three types different of the wood for all connections.

DOWEL DIAMETER 6 mm			
Point	**GL20H**	**GL24H**	**GL32H**
k1	0,80	0,76	0,7
k2	0,76	0,71	0,66
k3	0,76	0,75	0,7
DOWEL DIAMETER 8 mm			
k1	0,80	0,75	0,7
k2	0,77	0,7	0,66
k3	0,79	0,71	0,69
DOWEL DIAMETER 10 mm			
k1	0,80	0,76	0,7
k2	0,78	0,71	0,68
k3	0,78	0,73	0,69

10.3 ANNEX 3

Annex 3 represents the comparison of all key points external and internal within the same connection.

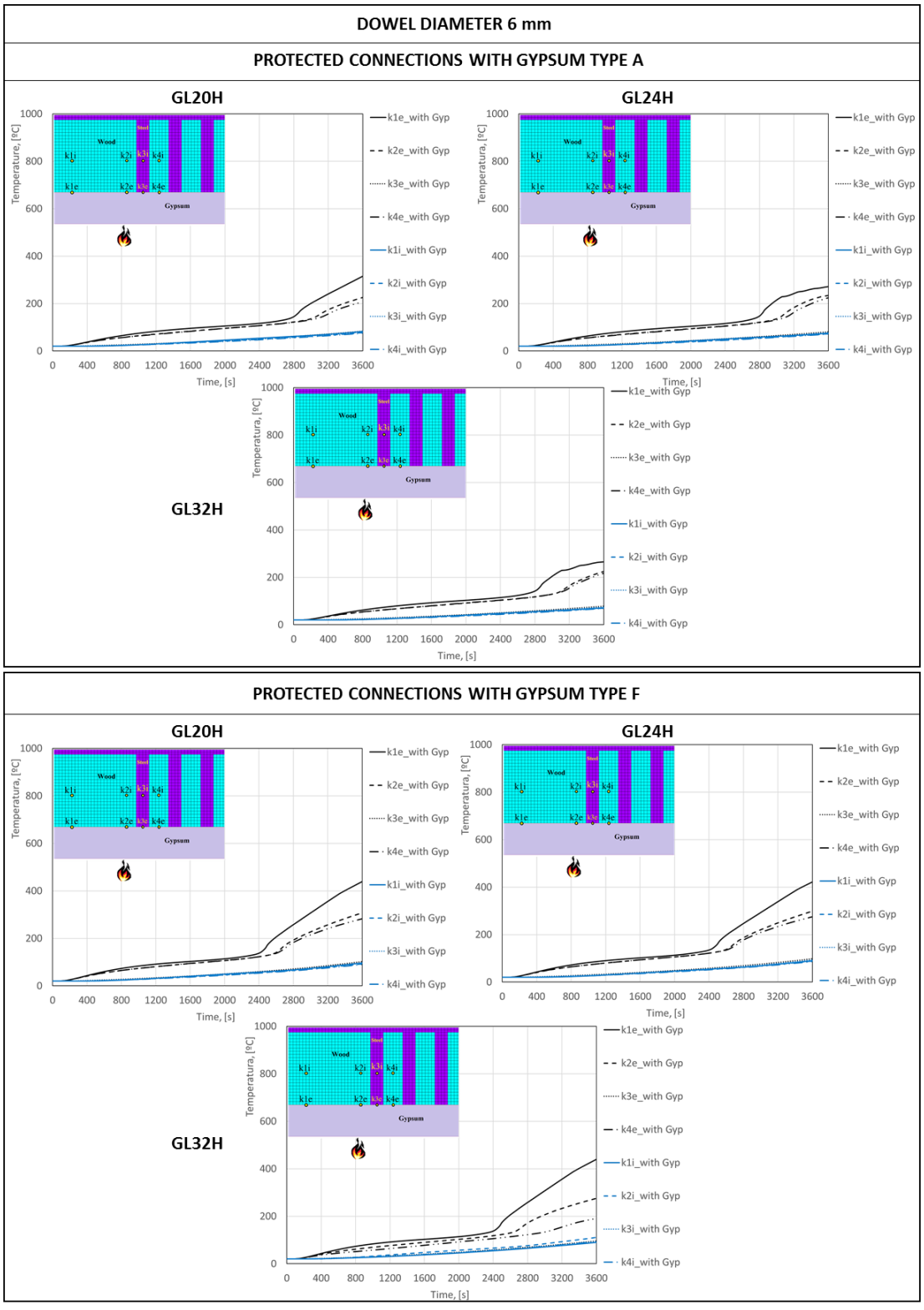

UNPROTECTED CONNECTIONS

GL20H

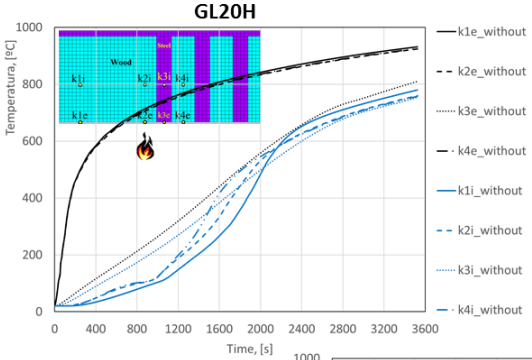

GL24H

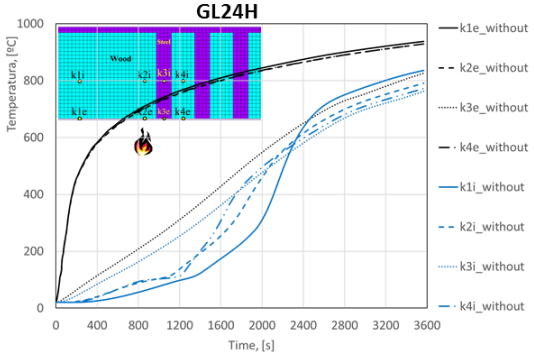

GL32H

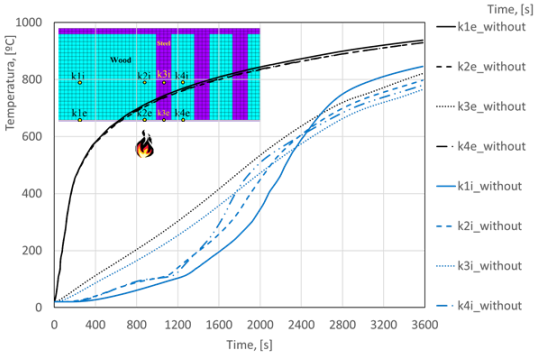

DOWEL DIAMETER 8 mm

PROTECTED CONNECTIONS WITH GYPSUM TYPE A

GL20H

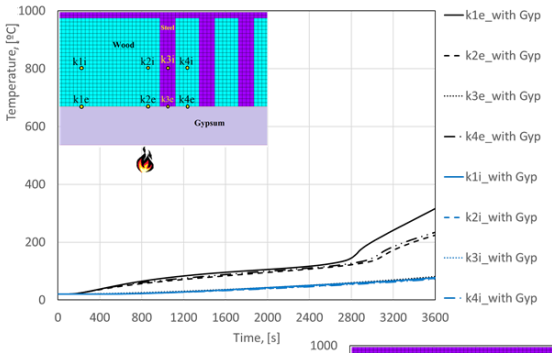

GL24H

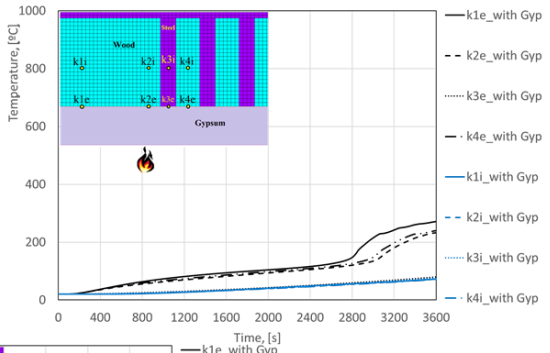

GL32H

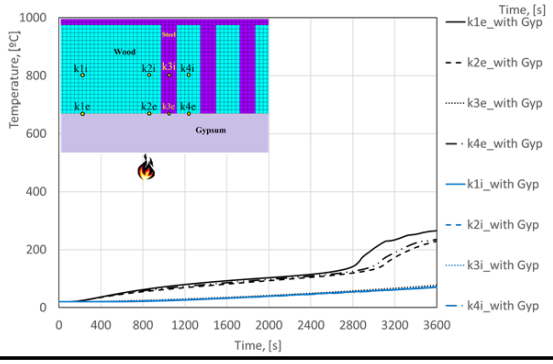

PROTECTED CONNECTIONS WITH GYPSUM TYPE F

GL20H

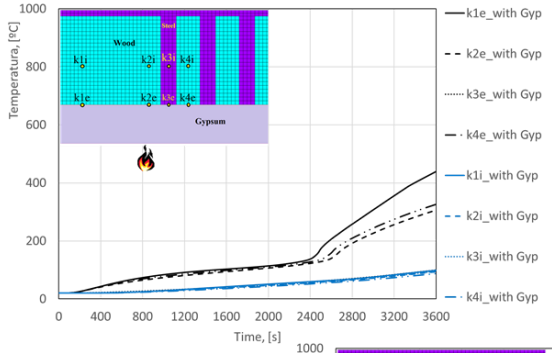

GL24H

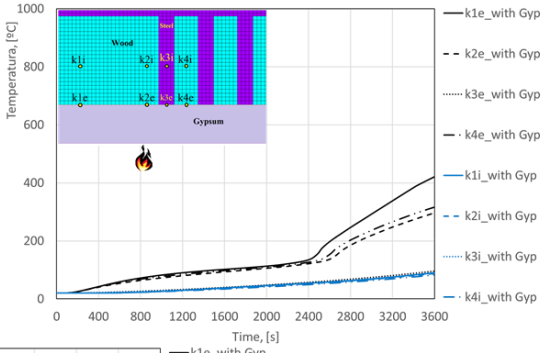

GL32H

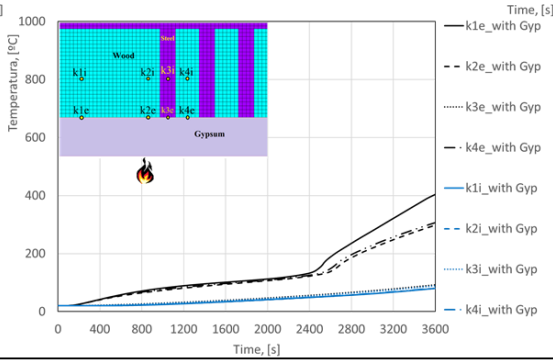

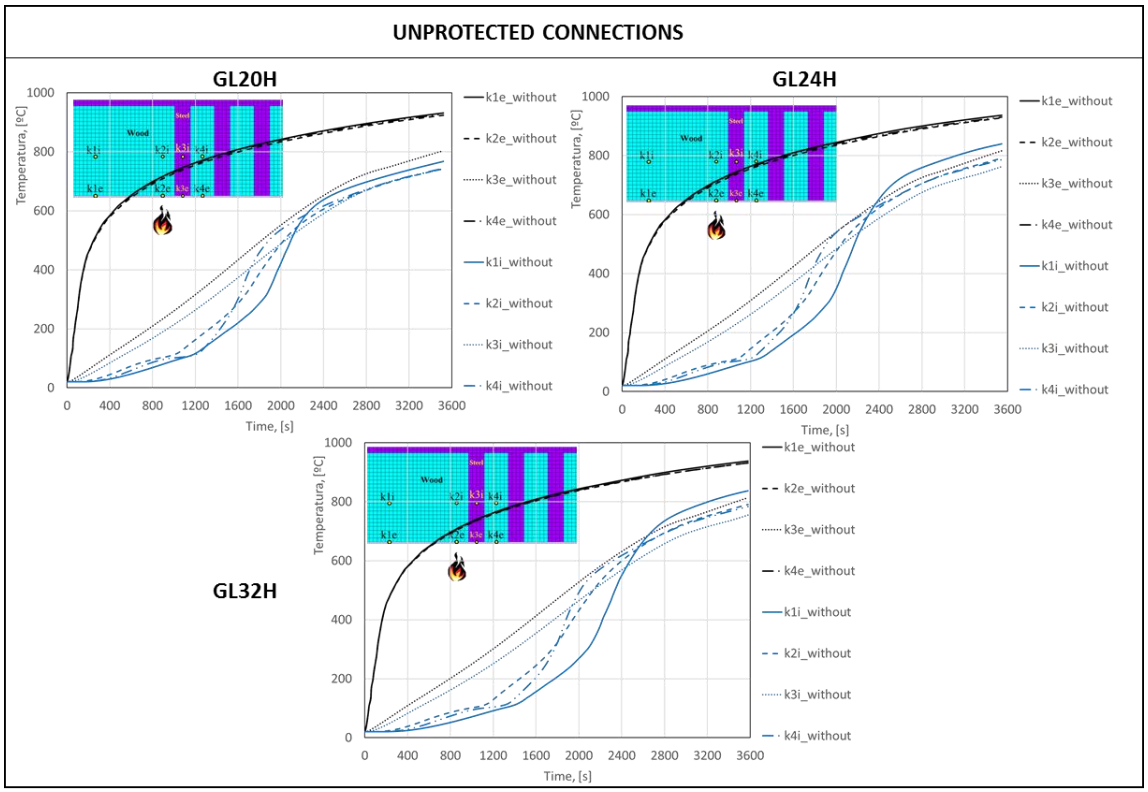
UNPROTECTED CONNECTIONS
GL20H
GL24H
GL32H
Temperatura, [ºC]
Time, [s]
k1e_without
k2e_without
k3e_without
k4e_without
k1i_without
k2i_without
k3i_without
k4i_without
Wood
Steel

DOWEL DIAMETER 10 mm

PROTECTED CONNECTIONS WITH GYPSUM TYPE A

GL20H

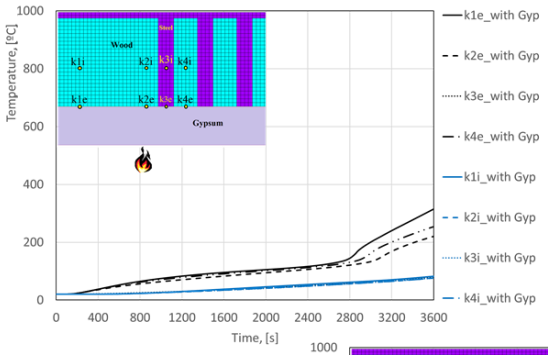

GL24H

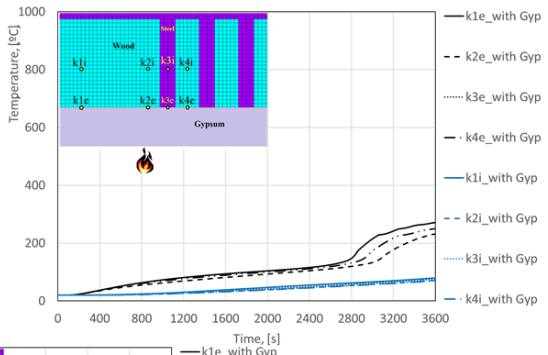

GL32H

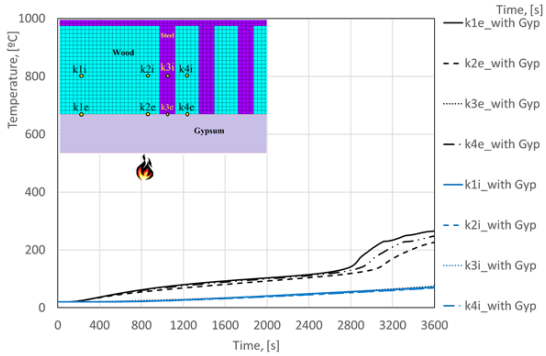

PROTECTED CONNECTIONS WITH GYPSUM TYPE F

GL20H

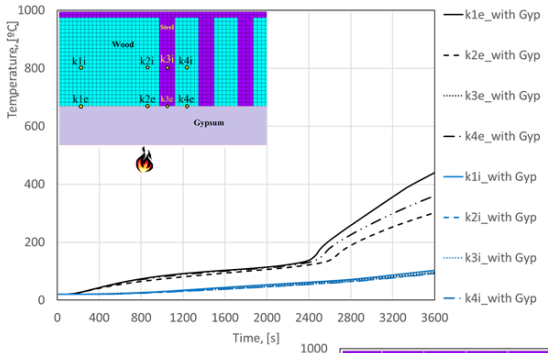

GL24H

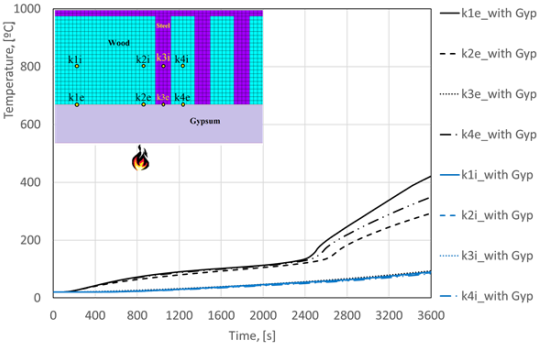

GL32H

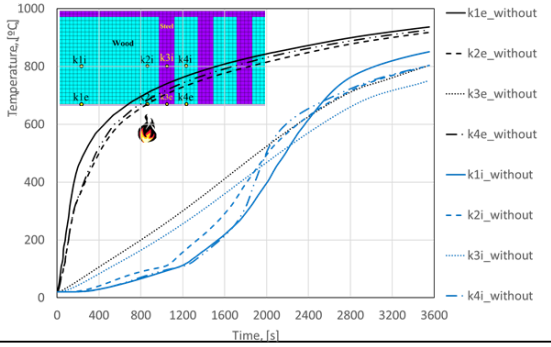

UNPROTECTED CONNECTIONS

GL20H

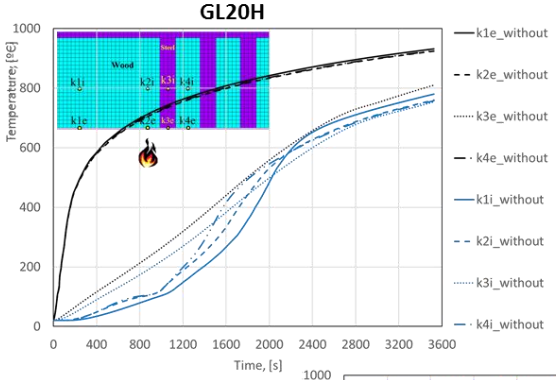

GL24H

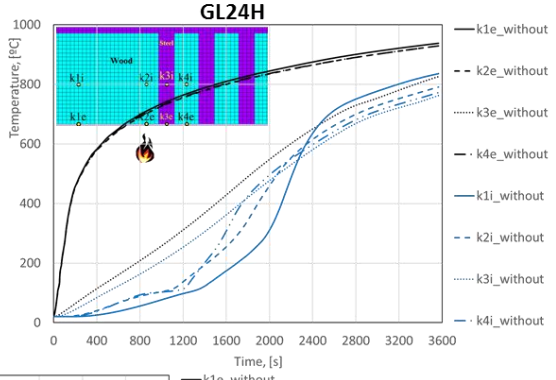

GL32H

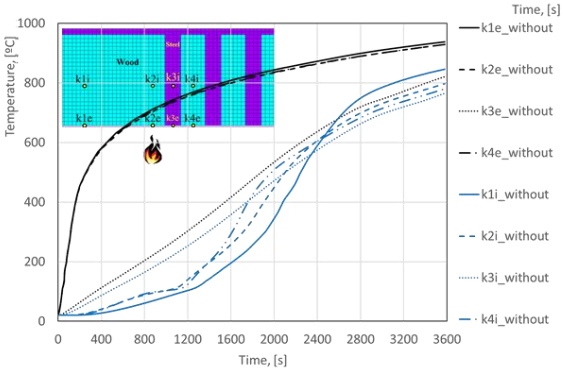

10.4 ANNEX 4

Annex 4 presents the numerical results of the temperature development at two different fire time instants (20 and 30 min) on all connections.

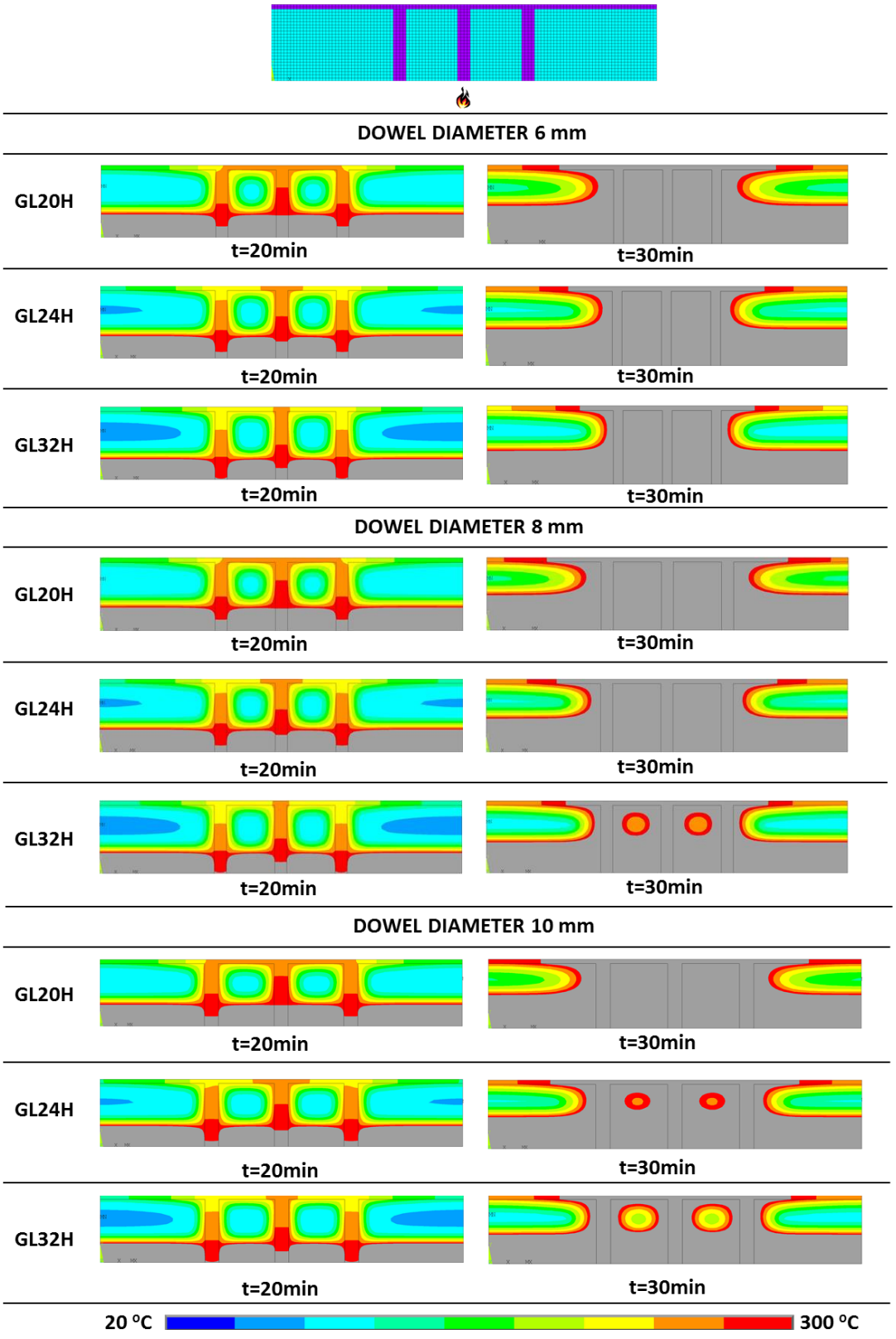

10.5 ANNEX 5

Annex 5 presents the numerical results of the temperature development at 60 minutes in the protected connection, comparing the two used gypsum types.

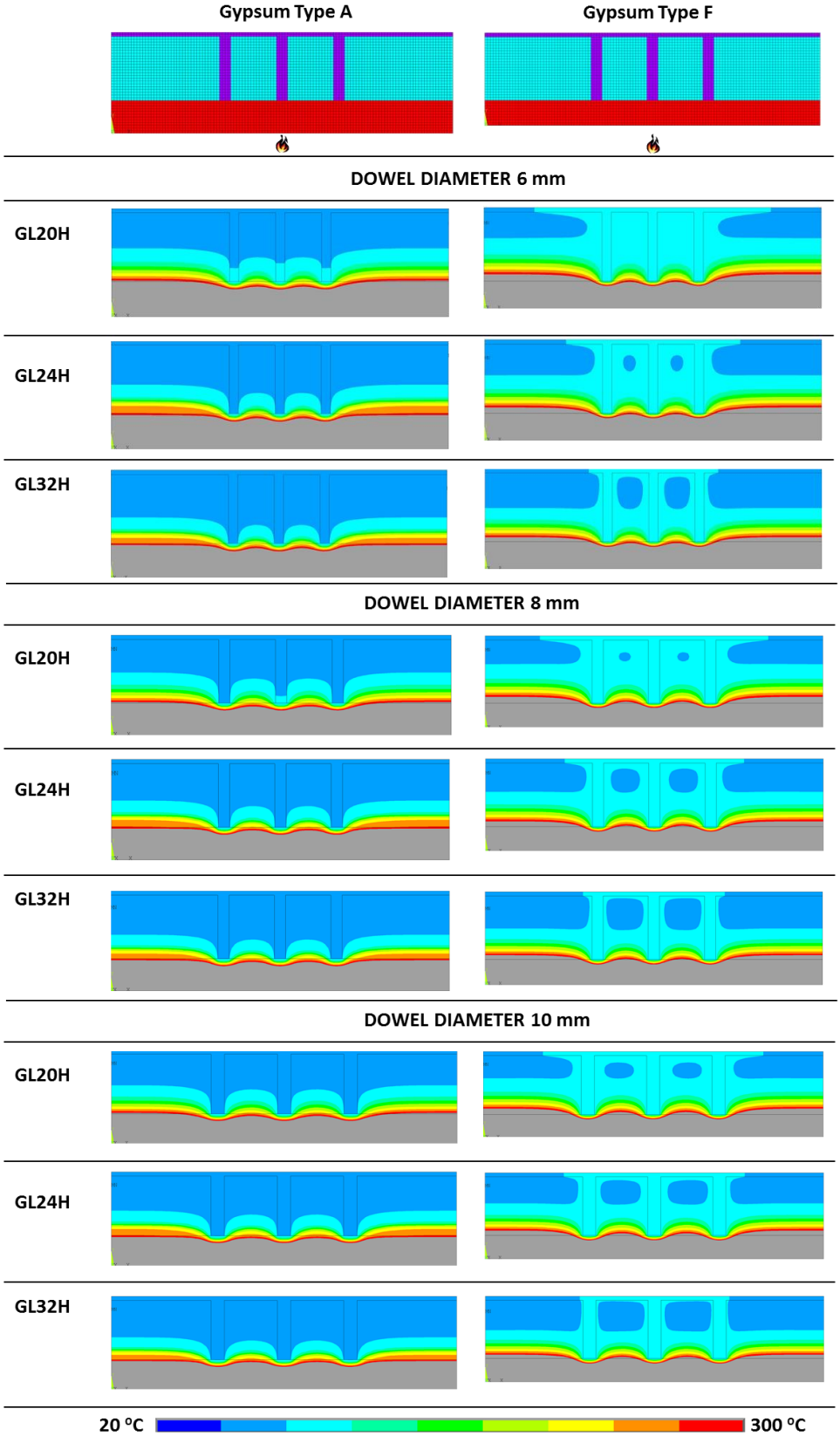

10.6 ANNEX 6

Annex 6 represents the comparison between the different types of gypsum used for all connections for both external and internal points.

DOWEL DIAMETER 6 mm

GL20H

EXTERNAL

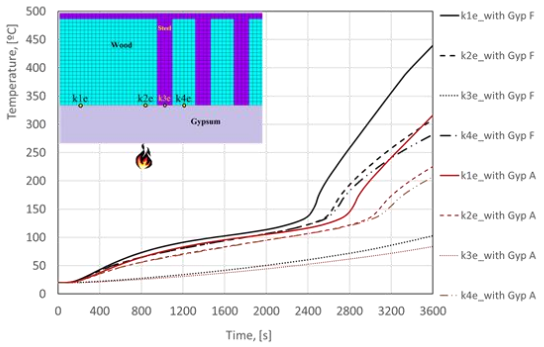

INTERNAL

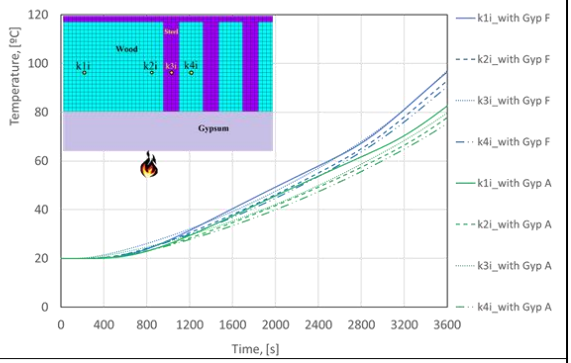

GL24H

EXTERNAL

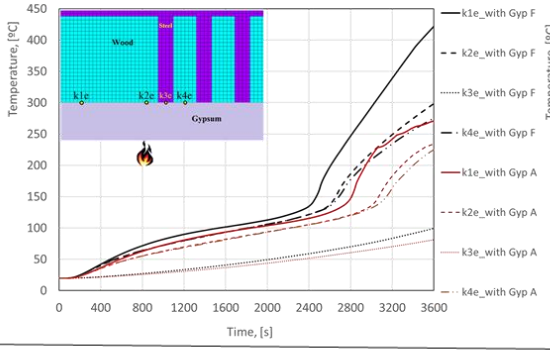

INTERNAL

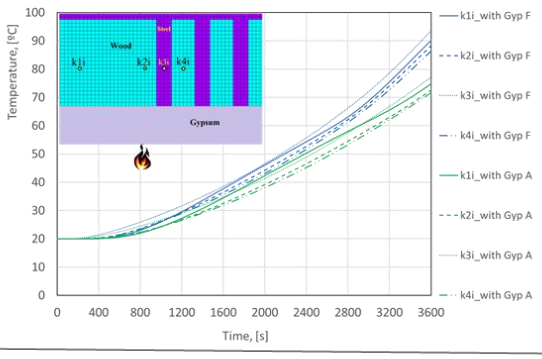

GL32H

EXTERNAL

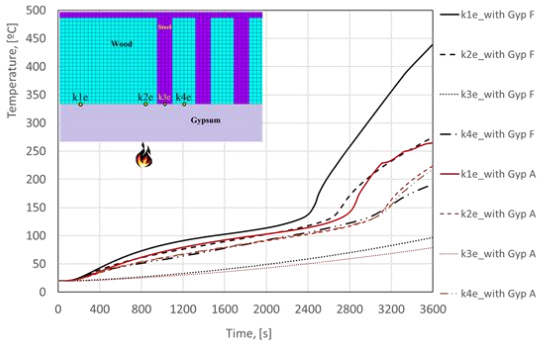

INTERNAL

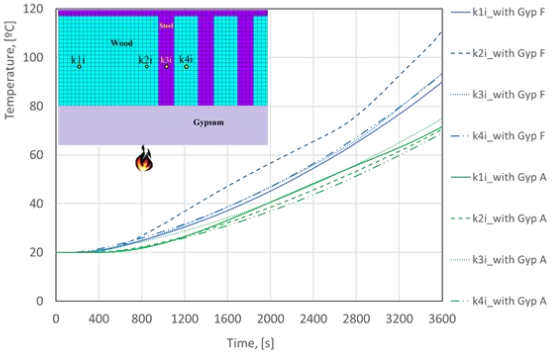

DOWEL DIAMETER 8 mm

GL20H

EXTERNAL

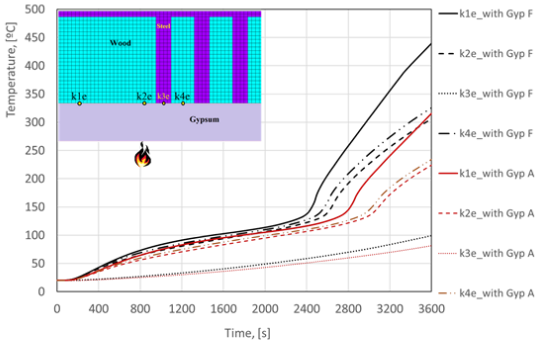

INTERNAL

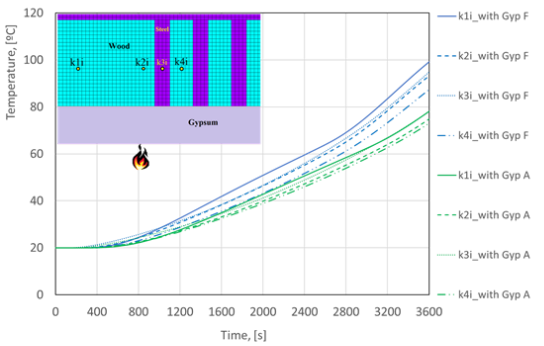

GL24H

EXTERNAL

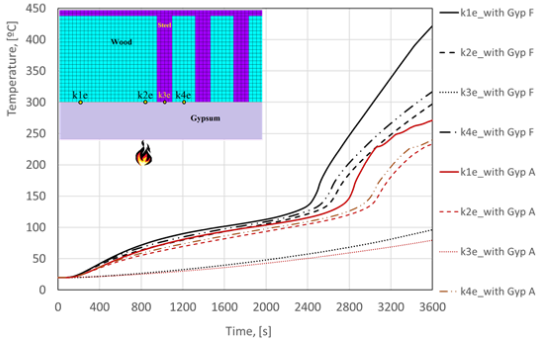

INTERNAL

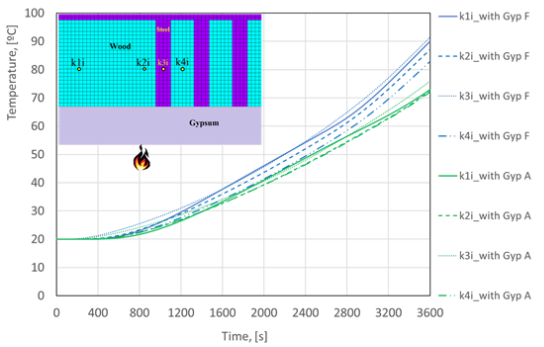

GL32H

EXTERNAL

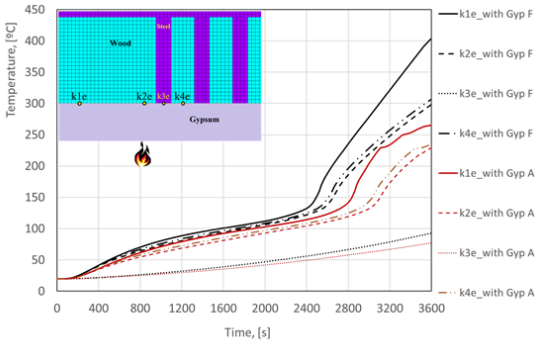

INTERNAL

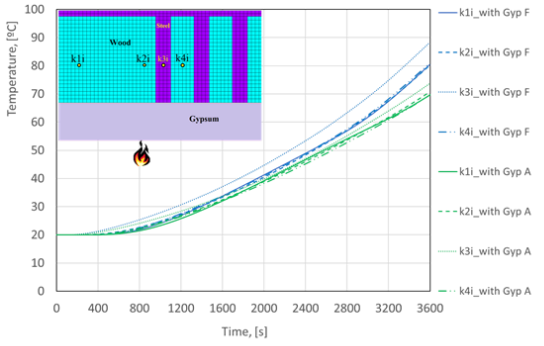

DOWEL DIAMETER 10 mm

GL20H

EXTERNAL

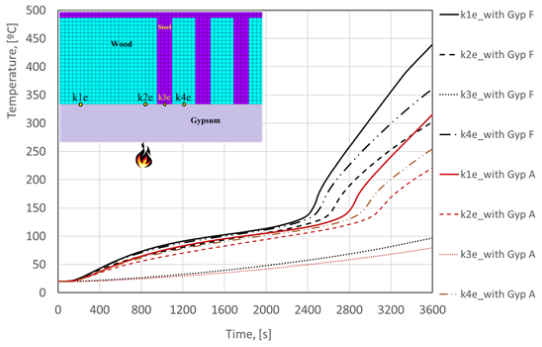

INTERNAL

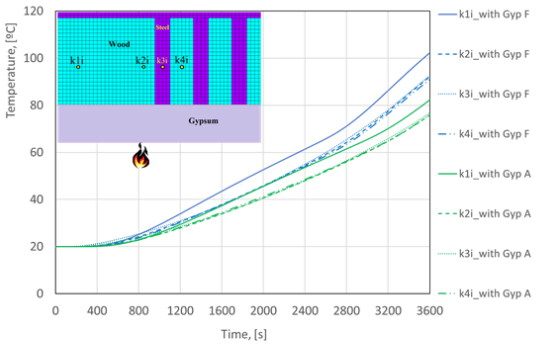

GL24H

EXTERNAL

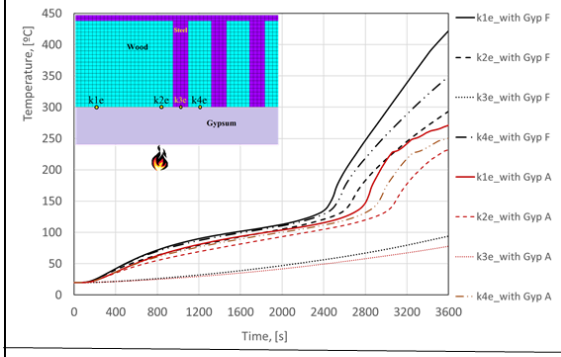

INTERNAL

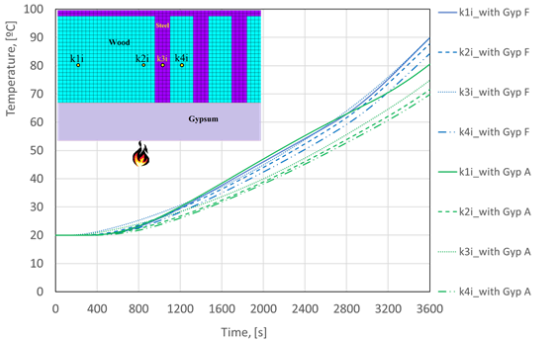

GL32H

EXTERNAL

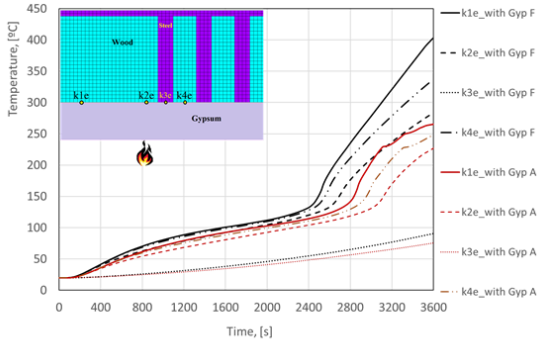

INTERNAL

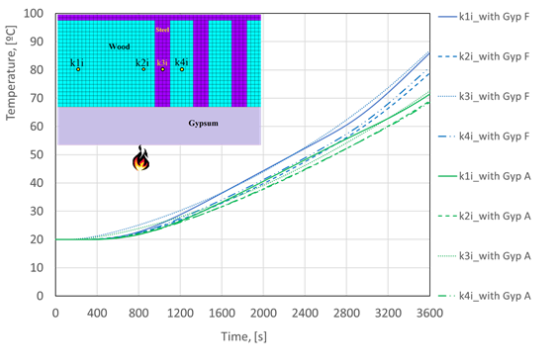

10.7 ANNEX 7

Annex 7 represents the comparison between the protected connection with gypsum type A and the unprotected connections for both external and internal points.

DOWEL DIAMETER 6 mm

GL20H

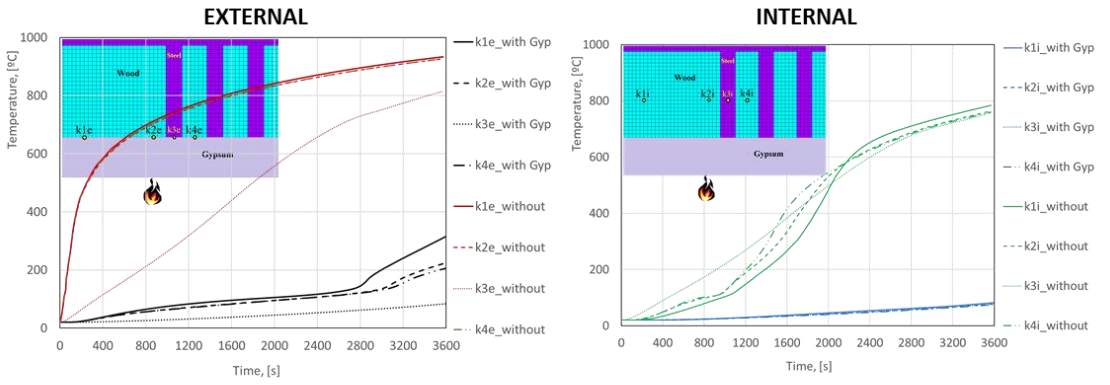

GL24H

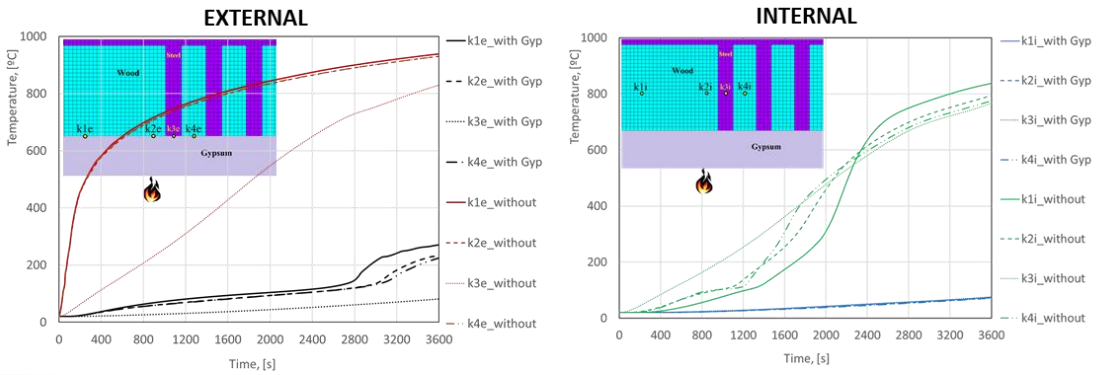

GL32H

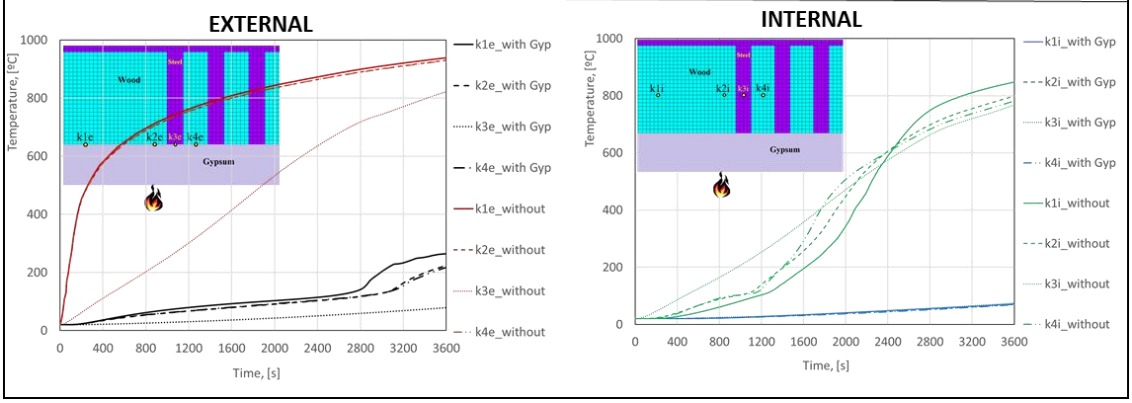

DOWEL DIAMETER 8 mm

GL20H

EXTERNAL

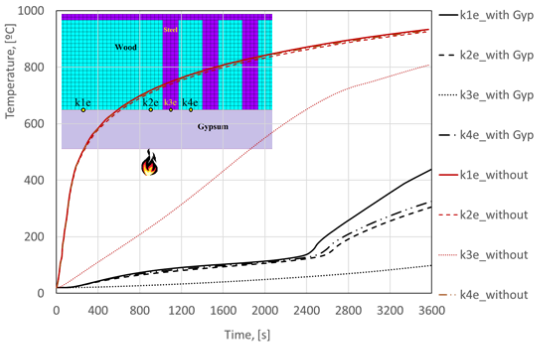

INTERNAL

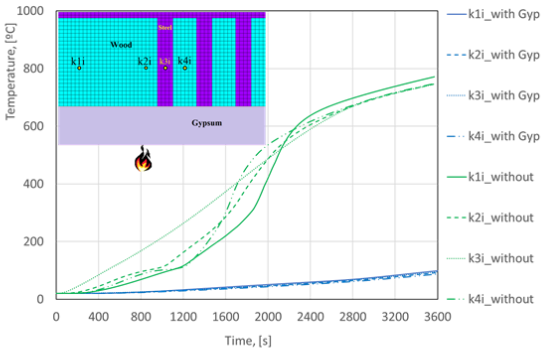

GL24H

EXTERNAL

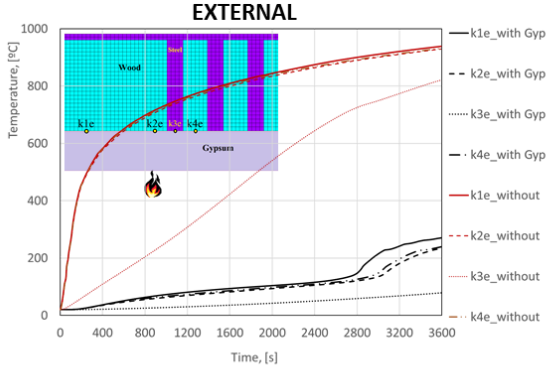

INTERNAL

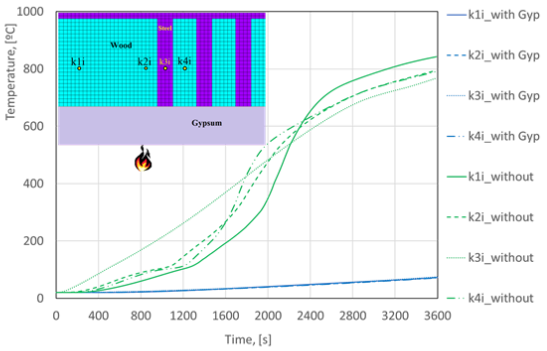

GL32H

EXTERNAL

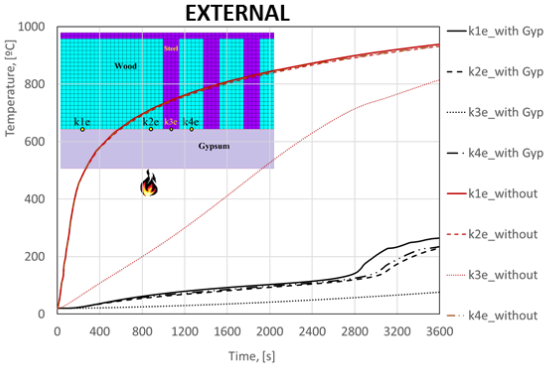

INTERNAL

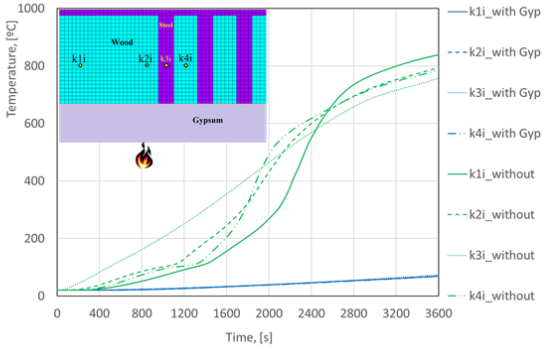

DOWEL DIAMETER 10 mm

GL20H

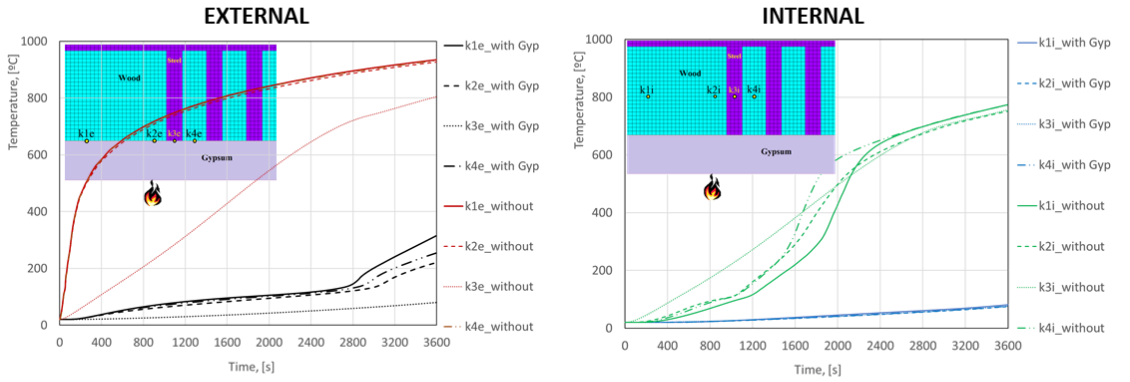

GL24H

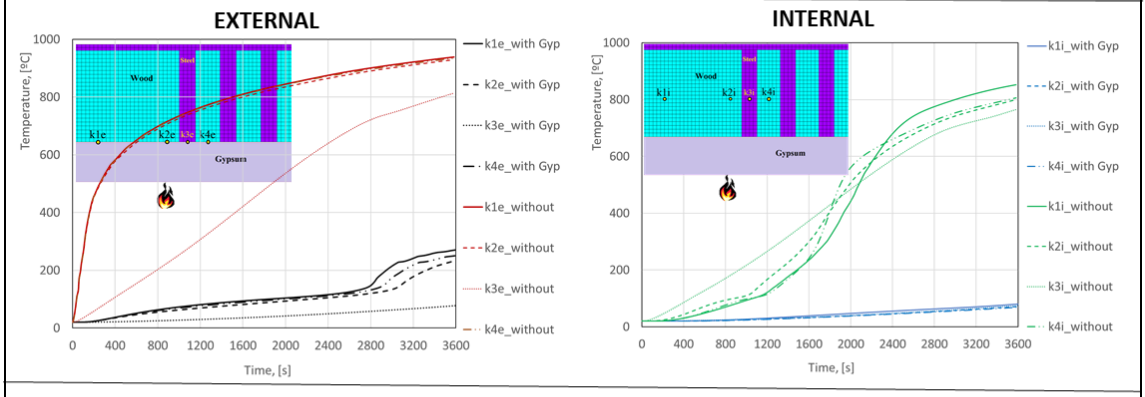

GL32H